Received: 27 January 2023 | Revised: 20 May 2023 | Accepted: 22 June 2023

DOI: 10.1002/eqe.3965

RESEARCH ARTICLE

WILEY

Seismic and energy upgrading of existing buildings—full-scale testing of retrofitted masonry-infilled RC frames

Chrysostomou Christis Z[1] | **Votsis Renos**[1] | **Kyriakides Nicholas**[1] | **Illampas Rogiros**[2] | **Filippou Christiana A**[1] | **Bousias Stathis**[3]

[1]Department of Civil Engineering and Geomatics, Cyprus University of Technology, Limassol, Cyprus

[2]Department of Civil Engineering, University of Minho, ISISE, Guimarães, Portugal, and at the Department of Civil and Environmental Engineering, University of Cyprus, Nicosia, Cyprus

[3]Department of Civil Engineering, University of Patras, Patras, Greece

Correspondence
Filippou Christiana A, Department of Civil Engineering and Geomatics, Cyprus University of Technology, Limassol, Cyprus.
Email: ca.filippou@edu.cut.ac.cy

Abstract

Taking into consideration the seismic vulnerability and the poor energy performance of the European building stock, and the increasing socio-economic and environmental need for integrating seismic upgrading with energy efficiency improvement, an experimental study involving the lateral load testing of full-scale one-story one-bay masonry infilled RC frames and load-bearing masonry walls was carried out in the framework of the SupERB research project aiming to investigate the efficiency of integrated seismic and energy upgrading systems. The integrated approach is based on the use of textile reinforced mortar (TRM) overlays combined either with traditional thermal insulation (extruded polystyrene, XPS) or with thermally efficient mortar incorporating phase change material (PCMs). The proposed integrated approach can be applied on the exterior face of the structure, so as to facilitate its application in real structures in the easiest possible way and with minimum disturbance to the inhabitants of the buildings. In this paper, only the structural performance of masonry-infilled RC frames retrofitted with the proposed integrated approach is presented, while the energy benefits will be presented in a separate paper. Thus, in this paper, the structural performance of an integrated seismic and energy upgrading approach was assessed through five full-scale one-story one-bay masonry infilled RC frames that were retrofitted with different schemes of TRM combined with thermal insulation materials subjected to in-plane displacement-controlled cyclic loading. The following parameters were investigated experimentally: the number of TRM overlays (one or two layers of TRM combined with thermal insulation), the use of thermally efficient PCM-enhanced TRM layer in contrast to the use of conventional XPS insulation, and different retrofitting configurations (placement of the TRM in a sandwich form over and/or under the novel or the traditional insulation). From the results obtained in this study, it can be

concluded that all energy and seismic upgrading systems examined have a positive impact on the response of the structural system to cyclic loading, with the ones with two layers of TRM having a better performance compared to the ones with one layer of TRM and all of them a better performance than the control specimen. The use of two layers of TRM cancels the drawback of infilled frames, which at very small drifts they reach their maximum capacity and after that they rapidly fall to the capacity of the bare frame, providing capacities above 80% of their peak capacity for drifts up to 2%. In all the tests the TRM whether it was combined with XPS or included PCMs contributed to a better distribution of the cracks in the infill and delayed premature brittle failures. The presence of the TRM had also the advantage that it remained intact throughout the tests preventing the fall of debris out of the plane of the infilled frame, both in the retrofitted and unretrofitted sides.

KEYWORDS
cyclic in-plane loading, energy and seismic retrofitting, full-scale testing, masonry-infilled RC frame, phase change material (PCM), textile reinforced mortar (TRM)

1 | INTRODUCTION

The vast majority of existing buildings in Europe are reinforced concrete (RC) frame structures with exterior masonry infills. Most of these buildings were constructed before the introduction of modern-day seismic design codes (e.g., Eurocodes) or energy performance regulations (e.g., energy performance of buildings directive [EPBD][1]). In fact, about 35% of the current European building stock has exceeded its initially intended service life (typically 50 years for structures of normal importance), 75% is energy inefficient and 70% is vulnerable to earthquake actions.[2] Substandard seismic detailing increases the risk for human casualties and high economic losses due to the damage of existing buildings under high- or moderate-intensity earthquakes. At the same time, energy deficient buildings are responsible for 35% of the total energy consumption in Europe and contribute 38% of greenhouse gas emissions globally.[3] Hence, there is an urgent socio-economic and environmental need in Europe for integrating seismic upgrading with energy efficiency improvement. This is a key aspect that will allow achieving acceptable levels of structural safety and will assist toward attaining the ambitious EU energy-saving and decarbonization goals.

In the past 5 years, research for the development of integrated seismic and energy retrofitting solutions has received increasing attention.[2,4] This has been largely incentivized by EU policies such as the Green Deal[5] and the Renovation Wave.[6] One promising hybrid approach for the integrated seismic and energy upgrading of existing buildings lies on the combined use of textile reinforced mortars (TRM) and thermal insulation materials. TRM composites consisting of non-corrosive multi-axial textile fabrics embedded in inorganic matrixes (lime- or cement-based mortars) have been studied extensively during the last decade and have proven to be quite effective for the seismic retrofitting of infilled RC frames[7–12] and masonry walls.[13] Specifically, the effectiveness of using the TRM to reduce either the out-of-plane collapse vulnerability of infilled frames or either the combined in-plane and out-of-plane damages of infilled frames was examined by Da Porto et al.,[13] Sagar et al.,[14] Minotto, et al.,[12] De Risi et al.,[15] and Furtado et al.,[16,17] while the effectiveness of using the TRM to increase the in-plane lateral capacity of infilled frames was investigated by Koutas et al.,[8] Akhoundi et al.,[10] and by Ismail et al.[18] Also, an overview description of the studies conducted so far to examine either numerically or experimentally the effectiveness of using the TRM for retrofitting masonry-infilled RC frames and masonry walls is presented in Filippou et al.[7] On the other hand, the installation of conventional (e.g., polyurethane, XPS—extruded polystyrene, EPS—expanded polystyrene, etc.), or smart insulation materials (e.g., capillary tube heating systems) has been proven to enhance energy performance by reducing significantly thermal losses through the building envelope.[19,20] The idea of creating a compact multilayer retrofitting solution combining TRM with insulation materials was first proposed in Triantafillou et al.[21] and Karlos et al.[22] who investigated this system's applicability on masonry walls subjected to out-of-plane and in-plane loading. Subsequently, several experimental and numerical studies were conducted to examine the

NOVELTY

1. Full-scale testing of simultaneous seismic and energy upgrading of structural systems.
2. Study of the use of a thermally efficient phase change material (PCM) in textile reinforced mortar (TRM) in contrast to the use of conventional extruded polystyrene (XPS) insulation combined with TRM.
3. Assessment of the application of the retrofitting only on the exterior face of the structure, so as to facilitate the application of the proposed methodology in real structures in the easiest possible way and with minimum disturbance to the inhabitants of the buildings.
4. Examination of different retrofitting configurations (placement of the TRM in a sandwich form over and/or under the novel or the traditional insulation).

performance of similar systems applied on RC and masonry members[22–24] and proof of concept regarding the effectiveness of such solutions has been provided.[21,25] A numerical study by Gkournelos et al.[23] concluded that the combined seismic and energy retrofitting of existing RC buildings can reduce seismic vulnerability and minimize the expected annual loss related to earthquake risks. Bournas,[25],[26] and Mastroberti et al.[27] reported that integrated retrofitting solutions are much more effective in economic terms compared to simple seismic or energy upgrading, as the initial investment is paid back faster. Pohoryles et al.,[28] assessed the effect of this combined retrofitting approach on the energy performance of the European building stock at macro level (city) considering different levels of seismic hazard and climatic conditions. The authors concluded that adequate retrofitting of the buildings' envelope could achieve reductions of about 70% in heating and cooling energy demand. Other researchers have investigated the use of prefabricated panels made of textile reinforced concrete (TRC) with embedded phase-change materials (PCMs) as a quick onsite intervention for enhancing the structural and thermal performance of building envelopes.[29,30] Further research on prefabricated TRC panels involves the inclusion of capillary tubes (TCPs) for improving energy performance and the implementation of quasi-static cyclic loading tests on infilled RC frames and masonry walls.[31] Despite intensified research efforts, seismic-plus-energy upgrading through a single intervention is a relatively new concept presenting several challenges that have not been addressed yet. Relevant solutions need to reach higher technological readiness level to enable extensive practical applications in the construction industry. A critical gap in the literature is the lack of adequate data describing the influence of such systems on the overall structural behavior of full-scale masonry-infilled RC frames. Instead, efficiency has been mainly evaluated based on small-scale tests (i.e., tests on RC beams or columns or masonry wallets alone) which may not always provide valid conclusions regarding the systems' response at the global structure scale.

In light of the above, an experimental study involving the in-plane load testing of full-scale one-story one-bay masonry infilled RC frames and load-bearing masonry walls was carried out in the framework of the SupERB research project aiming to investigate the efficiency of integrated seismic and energy upgrading systems. The integrated approach is based on the use of TRM overlays combined either with traditional thermal insulation, XPS, or with thermally efficient mortar incorporating PCMs. In that project a series of tests for examining the energy performance of various retrofitting solutions were also carried out, along with the formulation of a methodology for the selection of the best solution for integrated seismic and energy upgrading for a given structure. In this paper, the structural performance of masonry-infilled RC frames retrofitted with the proposed integrated approach will be presented, while the other results will be presented in separate papers.

The structural performance of an integrated seismic and energy upgrading approach was assessed through full-scale in-plane loading tests on retrofitted masonry-infilled RC frames. The retrofitting solutions hereby examined consist of TRM structural overlays combined with XPS panels applied on the exterior face of the structure, so as to facilitate the application of the proposed methodology in real structures in the easiest possible way and with minimum disturbance to the inhabitants of the buildings. Two types of TRM matrix materials were considered: (a) a conventional polymeric cement mortar and (b) a purposely developed cementitious mortar that incorporates PCMs, and exhibits enhanced thermal properties. Five quasi-static in-plane cyclic loading tests were carried out on masonry-infilled RC frames with different retrofitting schemes. Several parameters were experimentally investigated including the number of TRM overlays (one or two layers of TRM combined with thermal insulation), the use of thermally efficient PCM-enhanced TRM layer in contrast to the use of conventional XPS insulation, and different retrofitting configurations (placement of the TRM in a sandwich form over and/or under the novel or the traditional insulation). In the first part of the paper the experimental program is presented

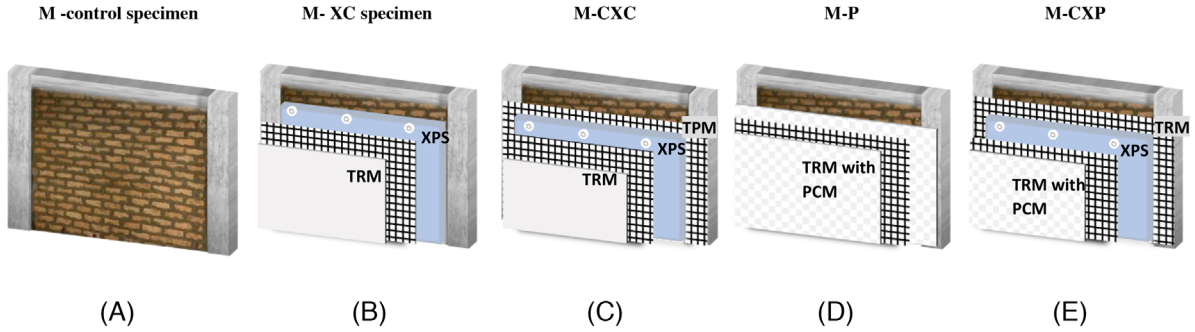

FIGURE 1 (A) Control specimen without retrofitting, (B) M-XC—Specimen retrofitted with one layer of XPS and with one layer of TRM, (C) M-CXC—Specimen retrofitted with one layer TRM, then with XPS, and with one layer of TRM, (D) M-P-Specimen retrofitted with one layer of TRM with PCMs, and (E) M-CXP-Specimen retrofitted firstly with one layer of TRM, then with one layer of XPS, and with one layer of TRM with PCMs.

and then the geometry and the materials of the test specimens, which is followed by the strengthening scheme, the test setup, and the instrumentation. Then the results are presented and discussed, a comparison among them is made and conclusions are drawn.

2 | EXPERIMENTAL PROGRAM

Five full-scale masonry-infilled RC frames were designed, built and tested under in-plane displacement-controlled cyclic loading. The first specimen was tested as-built and served as the control specimen (without TRM or insulation material), whereas the other four specimens were retrofitted with different schemes of TRM combined with thermal insulation materials as shown in Figure 1. In this study, for the TRM retrofitting layer, commercial glass fiber grid with alkali-resistant coating was used and it was binding with either conventional polymeric cement mortar, or with purposely developed cementitious mortar that incorporates PCMs. Besides the use of the PCM for energy upgrading, XPS insulation was also used. More details regarding the materials used for seismic and energy upgrading are presented in the next section. The retrofitting systems were applied only on one side of the infilled frames, so as to facilitate the application of the proposed methodology in real structures in the easiest possible way and with minimum disturbance to the inhabitants of the buildings. The notation of specimens consists of a series of letters as shown in Figure 1. The sequence of letters represents the sequence of the different materials in each specimen, starting from the infill wall and going outwards. The "M" refers to masonry-infilled RC frame, "C" stands for textile reinforced mortar (TRM) in which high-strength conventional polymeric cement mortar is used for binding the textile reinforcement, "X" refers to XPS insulation boards, and "P" stands for TRM in which purposely developed cementitious mortar that incorporates PCMs is used for binding the textile reinforcement. The control specimen is denoted as M. In addition to the rest of the parameters being kept identical between the five frames, construction of the infills by the same craftsmen and the use of a common loading protocol allow for the direct comparison and assessment of the effectiveness of the retrofitting methods examined in this study. The thickness of the XPS polystyrene was equal to 80 mm, and the thickness of one layer of glass-TRM, as measured in the laboratory, ranged from 10 to 12 mm.

2.1 | Geometry and materials of the test specimens

The geometry of the tested masonry-infilled RC frames is shown in Figure 2. Each infilled frame had a height of 2.95 m and a length of 3.6 m. The height and length of the infill walls was 2.45 and 2.80 m, respectively, yielding a length-to-height aspect ratio of 1.14 for the infill wall. The RC columns were of rectangular cross section 200 × 400 mm (with the long side parallel to the plane of the frame) as shown in Figure 2C. The RC beam (Figure 2D) was of T-section with cross-sectional dimensions 200 × 500 mm and a flange of width 2000 mm, to account for the effective width of a floor slab, and at the same time the axial load. The thickness of the flange was set to 300 mm in order to account for the combined weight of a 120 mm thick and 3.9 m wide slab of the prototype building, a superimposed static vertical load of 1.5 kN/m^2 and a live

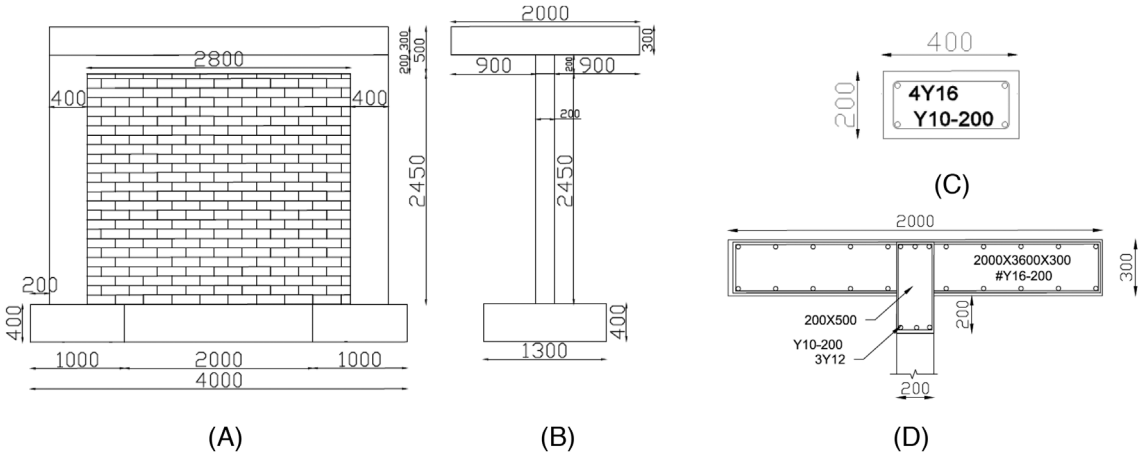

FIGURE 2 Geometry of the masonry-infilled RC frame (A) front view; and (B) side view, and reinforcement details of the (C) RC columns and of the (D) T-section RC beam (all dimensions in mm).

load of 1.5 kN/m^2. This resulted to a specimen slab with total weight of 6900 kg including the weight of actuators and their supports. This weight represents an axial load of 34.5 kN in each column for all the specimens. Although the RC beam (Figure 2D) was of T-section indicating an interior instead of an exterior frame, the proposed seismic and energy upgrading methodology is intended to be applied on the exterior face of the structure. The reason for selecting a T-section was mainly for providing a better stability of the specimen, and easier transfer of the load from the actuators to the specimen, and at the same time avoiding any torsional effects and out-of-plane moments that the L-shape beam would introduce. In addition, since this was a comparative study of four one-sided strengthened and insulated infilled-frames to the control specimen, any extra contribution of the T-beams was present in all five specimens, therefore the net effect was that of the contribution of the strengthening and the insulation.

The foundation of the masonry-infilled RC frames consisted of one RC foundation beam with dimensions equal to 2000 × 1300 × 400 mm as shown in Figure 2A,B, and of the foundation pads of each RC column with dimensions equal to 1000 × 1300 × 400 mm. For the construction of the RC columns and of the T-beam for all specimens C16/20 class concrete was used while for the foundation C30/37 class concrete was used (classification based on Eurocode 2). Compression tests performed on samples of C16/20 concrete 28 days after casting of each specimen gave mean compressive strength values ranging from 20 to 28 MPa. The respective results for the C30/37 concrete ranged from 39 to 44 MPa. The reinforcement detailing for the columns and T-section beam is presented in Figure 2C,D respectively, where the longitudinal reinforcement consisted of deformed bars, which had 16 mm diameter, and nominal yield stress equal to 500 MPa (class B500C). The RC foundation beam incorporated grid reinforcement composed of 16 mm bars with 200 mm spacing (Y16/200). Steel stirrups with diameter equal to 10 mm (class of S500) were used as transverse reinforcement for all concrete members as shown in Figure 2A,B. The transverse reinforcement for all concrete members consisted of deformed bars (class B500C) with diameter equal to 10 mm and with 90° hooks at the ends. The thickness of the concrete cover to stirrups was kept equal to 20 mm.

The construction of each RC frame was implemented in two stages. First, each RC column with its foundation pad were precast along with an RC foundation beam and were positioned in the laboratory (Figure 3A). Then, the T-beam above the columns was cast inside the laboratory (Figure 3B). The columns' foundation pads and the foundation beam were fixed on the laboratory's strong floor with vertical prestressed anchors and were connected together through horizontal prestressing rods. The RC foundation beam (with dimensions equal to 2000 × 1300 × 400 mm) remained fixed for all the masonry-infilled RC frame specimens. Details regarding prestressing are provided in the next section.

The construction of the masonry infill wall of each specimen commenced in the laboratory at least ten to twelve days after completing the T-beam casting. All courses of masonry units were built on the same day and the space left between the infill wall and the beam soffit, was filled with mortar as shown in Figure 3. The infill wall was constructed using perforated, fired clay bricks with dimensions 100 ×200 ×300 mm and with the perforations running parallel to the unit's length of 300 mm. The void ratio of the eight holes perforated fired clay bricks was equal to 0.54. The infill wall's final thickness was equal to the width of the columns (200 mm). The mean compressive strength of the bricks perpendicular to the perforations was equal to 2 MPa. The composition of the jointing mortar used between the bricks was cement:

FIGURE 3 Construction of masonry-infilled RC frame (A) placement of precast RC columns and foundation RC beam, (B) construction of RC T-section beam, and (C) building of masonry infill wall with detail of the last row of bricks.

lime: sand 1:2.5:8 by vol. Mortar mix design was based on the recommendations of the Cyprus National Annex to EN 1996-1-1 for mortars with a minimum compressive strength > 2.5 MPa at 28 days. The flexural and compressive strengths of the jointing mortar were determined in accordance with EN 1015-11 as 1.8 MPa (COV 8.6%) and 5.9 MPa (COV 3.2%), respectively. Its elastic modulus was determined as 5763 MPa (COV 3.9%) following compression tests conducted as per EN 13412. The thickness of the bed and the head mortar joints was approximately 10 mm.

Three diagonal compression tests were performed on brick masonry specimens measuring (thickness × width × length) 200 × 650 × 650 mm to determine the shear modulus and the shear and tensile strength of the infill wall. Using the ASTM E519 interpretation of the diagonal compression test which assumes a pure shear stress state in the center of the masonry specimen, the mean shear modulus was found to be 3000 MPa (COV 20%) and the mean shear strength was estimated as 1.37 MPa (COV 18%). It is noted that based on the assumption made by ASTM E519 method the tensile strength was equal to shear strength. Furthermore, four uniaxial compression tests on brick masonry specimens of stack-bonded prisms composed of four masonry units were performed as per ASTM C1314 to determine the masonry infill's compressive strength and modulus of elasticity perpendicular to the perforations of the bricks. The mean values of the compressive strength and elastic modulus obtained from uniaxial compression tests are 3.6 MPa (COV 9%) and 6236 MPa (COV 33%), respectively. It is noted that in the calculation of the masonry properties hereby reported the net cross-sectional area of the masonry units was used.

2.2 | Strengthening scheme

Five masonry-infilled RC frames retrofitted with different schemes of TRM combined with thermal insulation materials were tested in this study as described in Figure 1. For the TRM retrofitting layers, a commercial glass fiber grid (Sikawrap-350G grid) with alkali-resistant coating was used. The grid has a mesh size equal to 18.1 mm × 14.2 mm and is provided in rolls 1000 mm wide. According to the data sheet provided by the producer, the coated grid has an area density of 360 g/m^2 and its tensile strength is 77 kN/m in the wrap direction and 76 kN/m in the weft direction. The elastic modulus of the dry glass fibers composing the grid is 80 GPa. The properties of the glass textile are summarized in Table 1.

Two types of mortar were used for binding the textile reinforcement in the construction of the retrofitting TRM overlays; conventional polymeric high-strength cement mortar[33] (referred to as conventional mortar), and a purposely developed cementitious mortar that incorporates PCMs with 20% w/w ratio of the solid constituents (referred to as PCM-enhanced mortar). The PCM-enhanced mortar was developed in the framework of the SupERB project and offers lower thermal conductivity compared to the conventional one as well as improved specific heat capacity and thermal diffusivity.[34] The adopted water-to-solid mixing ratios were 0.16 for the conventional mortar and 0.24 for the PCM-enhanced mortar. In both cases a consistency of 165 ± 5 mm was achieved. The compressive and flexural strengths of the hardened mortar materials were determined as per EN 1015-11 and their elastic modulus as per EN 13412. The conventional mortar gave a compressive strength of 64.4 MPa (COV 4.6%), a flexural strength of 8.6 MPa (COV 9.4%), and an elastic modulus of 31.2 GPa (COV 5.1%). The PCM-enhanced mortar had lower mechanical properties: compressive strength 14.4 MPa (COV 2%), flexural strength 4.8 MPa (COV 8%), modulus of elasticity 4.44 GPa (COV 3%). The conventional mortar (C) was used for specimens M-XC, M-CXC and the first layer of M-CXP, and the PCM-enhanced mortar (P) was used for specimen M-P and in the second TRM layer of specimen M-CXP (see Figure 1).

TABLE 1 Properties of the glass-textile reinforcement (Sikawrap-350G grid).

Glass-textile (Sikawrap-350G grid)	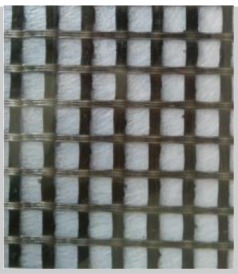
Mesh size (midroving to midroving grid spacing)	18.1 mm × 14.2 mm
Weight	360 g/m^2 (net 280 g/m^2)
Fiber density	2.6 gr/cm^3
Fiber's Tensile strength	2600 N/mm^2
Fiber's modulus of elasticity	80,000 N/mm^2
Tensile strength of the textile	76–77 KN/m
Rupture strain of the textile	3.45%–4.10%

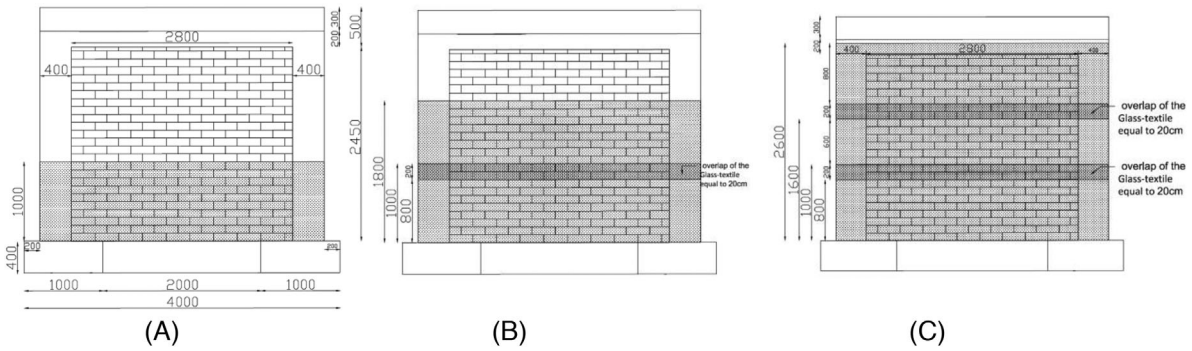

FIGURE 4 Overlapping of textile reinforcement: (A) first strip of textile reinforcement, (B) second strip of the textile reinforcement by overlapping the first strip by 20 cm, and (C) third strip of the textile reinforcement by overlapping the second strip of the textile by 20 cm.

The TRM retrofitting layer were applied only on one side of the specimens. Since the width of the textile reinforcement was equal to 1 m, the glass-textile reinforcement was applied with an overlap of about 0.20 m at the height of 0.80 m and of 1.60 m from the bottom of the infill wall as shown in Figures 4B,C, respectively. The 0.20 m overlapping length was in the range of 0.15–0.30 m used in relevant past experimental studies.[8,35,36] Thus, in this study three strips of textile were applied horizontally to the infilled frame to cover its height. The TRM retrofitting layers were applied using the wet lay-up technique and included the following steps (Figure 5).

1. A thin layer of mortar of about 5 mm was applied either on the infill wall or on the XPS insulation boards on the side of the infill to be retrofitted, on the short faces of the columns (200 mm) and on the long faces of the columns (400 mm), in the unretrofitted side of the wall, up to the installation height of the first textile strip (1 m) as shown in Figure 5.
2. The first strip of the textile was installed while the first layer of mortar was still fresh and was pressed firmly with a smooth spreader to make sure it was completely impregnated with the fresh mortar.
3. While the first layer of mortar was still fresh, a second layer of mortar was applied until the reinforcing textile was fully incorporated and any underlying voids were filled. The second layer of mortar was applied up to a height of 80 cm of the textile strip to enable 20 cm lengthways overlapping with subsequent textile strips.
4. The above procedure was repeated for the installation of subsequent strips of textile until the entire height of the specimen was covered.

The end thickness of each TRM layer was equal to 10–12 mm. Curing of the mortar was achieved in laboratory conditions. As shown in Figure 5, the TRM was applied on one side of the specimen by completely covering vertically the

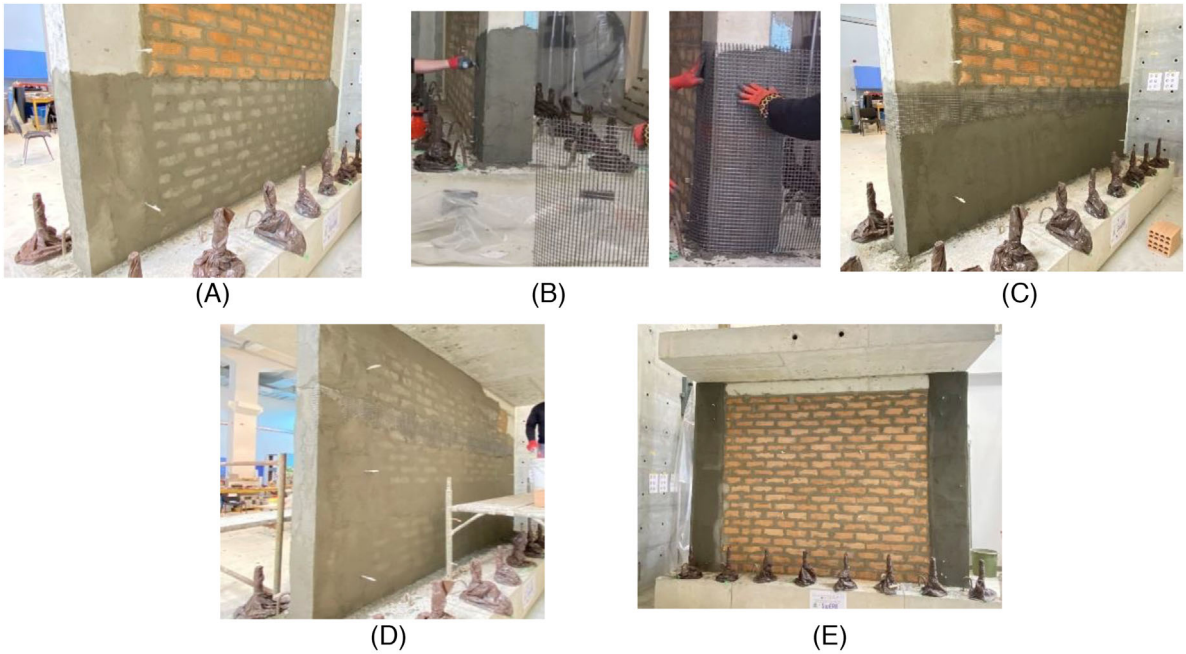

FIGURE 5 TRM Strengthening scheme application steps: (A) application of a first strip of the first layer of the mortar on the face of masonry infill and on the RC columns, (B) application of a first strip of the textile reinforcement on the short face of the column, (C) application of first strip of the second layer of the mortar on the face of masonry infill and on the RC columns, (D) application of a third strip of the first layer of the mortar on the face of masonry infill and on the RC columns, and (E) application of third strip of the textile reinforcement and the mortar on the short and long face of the column (back side of the specimen).

clear height of the infill wall and extending it to the outside short face of the columns (200 mm) and to the long faces of the columns (400 mm) on the unretrofitted side. It should be underlined that wrapping of the textile around the column sections is intended to provide sufficient anchorage, which is critical for achieving acceptable structural performance.

The application of the TRM in the test specimens, as it was explained above, was to represent the real-life application of the proposed integrated approach where the TRM will be wrapped externally around the building, which is critical for achieving the retrofitting targets and contributing to preventing the out-of-plane failure of the infills. This is achieved by providing circumferential confinement by increasing the hoop stresses. Adequate anchorage length should be provided at places where a connection should be made. The placement of the connections should be decided based on the expected stress concentration areas and should be away from the corners of the building. A length of 1.0–1.5 m is considered to be adequate, although further tests should be performed to quantify this length.

In this study, besides the use of PCMs as a thermal insulation material, XPS thermal insulation boards were also used which were externally applied on one side of the M-XC, M-CXC, and M-CXP specimens. XPS boards 80 mm thick and measuring 2500 × 600 mm were used. Four and a half boards were used in each specimen to completely cover the clear height of the infilled frame. According to EN 1364:2012 the XPS used in this study has the following characteristics: R = 2.30 m^2K/W and thermal conductivity coefficient λ = 0.035 W/mk. Installation of the XPS boards on either the infill wall or the TRM retrofitting layer was carried out using a suitable cement-based adhesive mortar as presented in Figure 6. The XPS polystyrene boards were applied either on the infill wall or on the TRM retrofitting layer using a suitable cement-based adhesive mortar (TSIRCO THERMOSTIC) applied at the surface of the polystyrene using a notched trowel (Figure 6A), and after the adhesive was dried out standard plastic dowels were placed through the insulation layer into the infill wall (Figure 6D). The adhesive was applied to the two sides of the XPS polystyrene boards aiming to prevent the delamination at the infill wall-polystyrene interface and at the TRM-polystyrene interface (Figure 6A,E).

2.3 | Test setup and instrumentation

All masonry-infilled RC frame specimens were subjected to a sequence of cycles of predefined displacement as shown in Figure 7. A cyclic displacement history (Figure 7) was applied in the middle of the slab of each specimen which corresponds

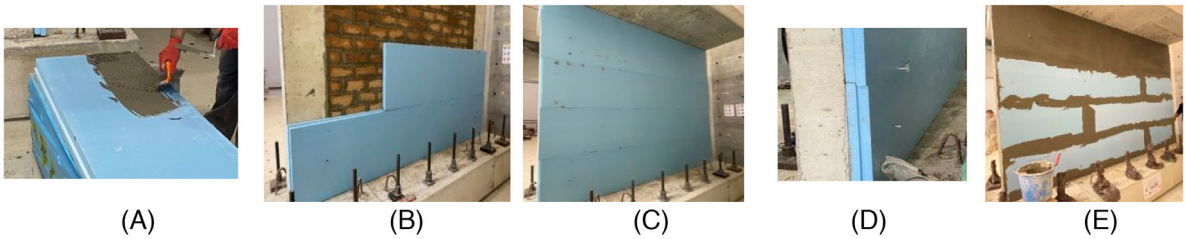

FIGURE 6 XPS boards application steps (A) adhesive material at the surface of the XPS using notched trowel, (B) application of the first and second strips of XPS board, (C) infilled frame with four and half XPS boards, (D) application of special plastic dowels, and (E) adhesive material at the surface of the XPS using notched trowel.

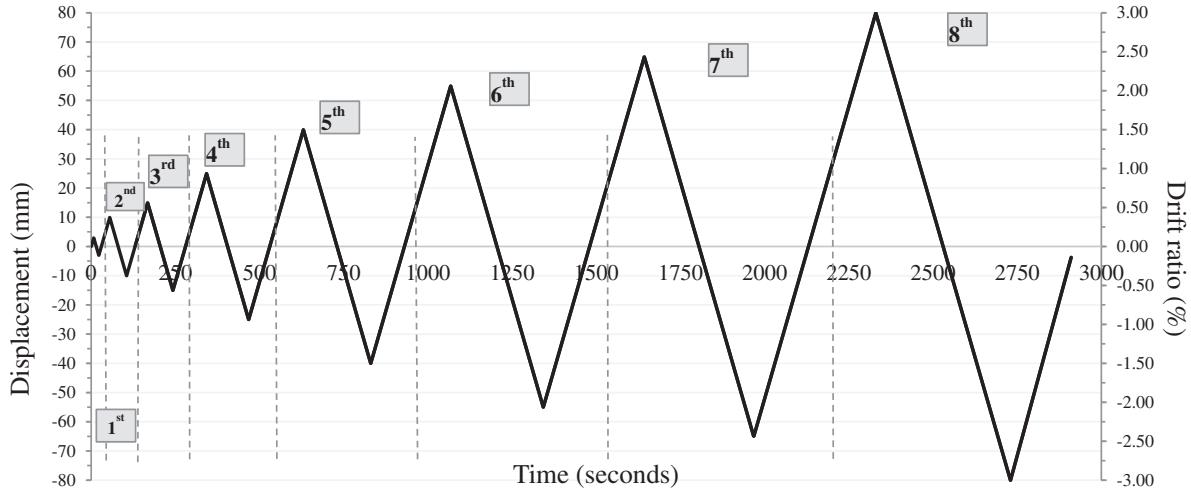

FIGURE 7 Displacement history.

to a story height of 2.8 m (Figure 8). Since the test specimens comprise of a single story, the drift ratios (i.e., imposed displacement divided by the story height) reported in Figure 9 and the rest of the paper, represent both the top story drift ratio and the inter-story drift ratio. Six cycles of loading were applied to the control specimen M, seven and a half cycles to the M-CX and the M-CXC specimens, six cycles to the M-P specimen, and eight cycles to the M-CXP specimen. The number of cycles imposed on each specimen was dictated by the degree of damage observed during the test, which was the determining factor for termination of the test for safety reasons. The rate of displacement loading was equal to 0.2 mm/min and the maximum displacement at the 8th cycle was equal to ±80 mm (±2.85% drift ratio). The drift ratios corresponding to each of the eight cycles are 0.11%, 0.35%, 0.53%, 0.89%, 1.43%, 1.96%, 2.32%, and 2.85%.

The test setup is shown in Figure 8. Figure 8 also shows the positive and negative direction of loading which represents the positive and negative displacements presented in Figure 7. Two servo-hydraulic actuators of 500 kN capacity were mounted on the specimens, one per side. The force and the displacement of the actuators were monitored by built-in load cells and transducers. Sixteen prestressing anchors were placed to fix the foundation (RC foundation beam and columns' foundation pad) to the laboratory's strong floor as shown in Figure 8. The vertical post-tensioning applied to the anchors at the column's foundation pad was equal to 250 kN, while the vertical post-tensioning applied to the anchors at the RC foundation beam was equal to 150 kN. Also, horizontal post-tensioning equal to 200 kN was applied to the foundation through a system of two steel transverse rods, as shown in Figure 8, in order to provide continuity between the column's foundation pad and the foundation beam. A system of two transverse rods with a diameter of 32 mm was used to fix the system of the actuator supports to the slab as shown in Figure 8. The post-tensioning for each of these transverse rods was equal to 350 kN. It is important to mention that an axial load of 69 kN was considered for all the specimens. This load is resulting from the weight of the slab of the T-section beam and the weight of the actuators and their supports, and it is shared equally by the two columns of the frame.

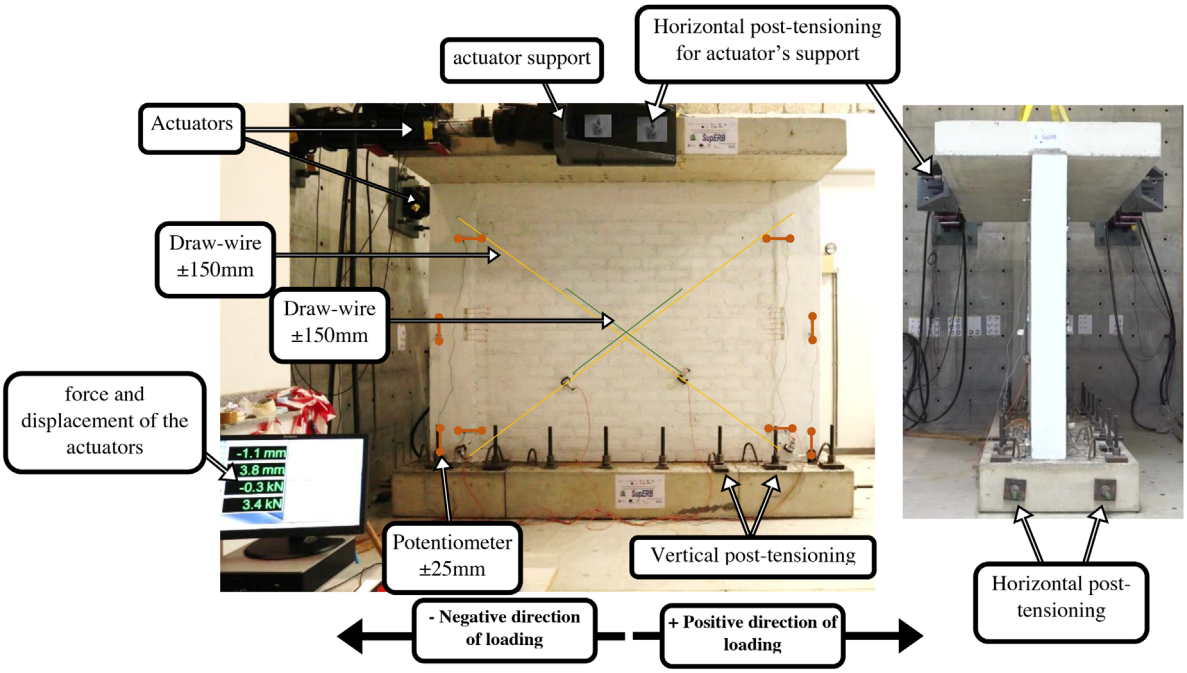

FIGURE 8 Test setup: Front view and side view.

For the purpose of this experimental program, a network of potentiometers, LVDTs, and draw wires was used to monitor the separation, the sliding, and the deformations of the diagonals of the infill walls and the deformation of the RC columns. The instrumentation layout used in each specimen includes the following:

1. A network of 8 potentiometers at selected locations of the unretrofitted side of each specimen, as shown in Figure 8 monitoring the separation at the interfaces of the infill wall to the surrounding frame members, and the axial deformations of the bounding RC columns.
2. A network of 7 LVDTs at selected locations of the retrofitted side of each specimen, monitoring separation at the interfaces between the infills and the surrounding RC frame members and the movement of the foundation of the wall relative to the strong floor.
3. Four draw wires at the diagonal of the unretrofitted infill wall, as shown in Figure 8 (indicated with yellow and green lines), monitoring the deformations of the diagonals of the infill wall.

Damage evolution was monitored using digital cameras.

3 | RESULTS AND DISCUSSION

Prior to the implementation of in-plane cyclic loading tests, free vibration tests were performed on each specimen in order to determine their dynamic characteristics (frequencies). The scope of testing was to examine the effect of the infill wall to the dynamic characteristics (frequencies) of the bare frame, and to examine also the effect of the different retrofitting schemes to the dynamic characteristics of the infilled frame. The free vibration tests performed used measurements of the free structural response after the application of an impact. The data were captured using a wireless acquisition system and two wireless accelerometers that were placed at the top section of each column. The impacts were executed on the loading RC beam using a rubber hammer and the captured decay response was processed and analyzed in a commercial signal analysis software. The fundamental period and frequencies of each specimen (including the bare frame) as obtained from the free vibration tests are summarized in Table 2. From Table 2 it is observed that the presence of the infill wall in the RC frame influences its dynamic characteristic, since the fundamental period of the infilled frame is three times lower than that of the bare frame. This was expected as the addition of the masonry wall in RC frames substantially increases the stiffness of the system, thus resulting to lower periods of vibration. It is also observed that the fundamental period of

TABLE 2 Fundamental period of the bare frame, of the control specimen (M), and of the M-XC, M-CXC, M-P and M-CXP specimens.

Specimen	Period (seconds)	Frequency (Hz)
Bare frame	0.105	9.52
M-control specimen	0.033	30.3
M-XC	0.028	35.7
M-CXC Measured at second layer of TRM	0.026	38.5
M-P	0.030	33.3
M-CXP Measured at the second layer of TRM	0.028	35.7

the retrofitted infilled frame with any retrofitting scheme is decreased by about 20% compared to that of the unretrofitted one. This indicates a further, but smaller, increase in the stiffness of the system, which, given the relatively low stiffness of the XPS insulation boards, it can be primarily attributed to the addition of TRM overlays.

Hereafter, the results of the cyclic loading tests are discussed on the basis of the recorded base-shear versus in-plane displacement response. The discussion also refers to the observed progression of cracking damage and to the failure mechanisms that occurred.

To examine the parameters influencing the proposed integrated retrofitting system a 2D finite element (FE) numerical model of the tested specimens of this study must be developed. The RC frame and the infill wall may be modeled as plane-stress elements with appropriate material models including their nonlinearity. It is important to also model the infill-frame interface with a Coulomb Friction model to capture the interface behavior. The TRM may be modeled also with plane-stress element following a macro-modeling approach and simple material models.[37] The results of the free vibration test as presented in Table 2 may be used for the correct implementation of the FE numerical models' characteristics. More details regarding the development of a FE numerical model of masonry-infilled RC frames with and without TRM may be found in Filippou et al.[38–41]

3.1 | M-control specimen

The control specimen was subjected to six cycles of displacement-controlled loading which resulted to a maximum imposed displacement of ±55 mm (±1.96% drift ratio). Figure 9 presents the base-shear force in relation to the top-displacement (hysteresis curve) and the progression of cracking at the front side of the specimen for the second, fourth and sixth cycles of loading. The maximum base-shear force was attained during the second cycle of loading at corresponding top-displacement of +9.9 mm (drift ratio of +0.35%), in the positive direction and is equal to +335 kN. In the negative direction the maximum base-shear force was recorded during the third cycle of loading corresponding to a top-displacement of −15 mm (drift ratio of −053%) and is equal to −309 kN. The peak base-shear and the peak drift ratio in each cycle of loading for all the specimens are presented in Table 3 for the benefit of the reader. During the second cycle of loading minor cracks formed at the lower right corner of the infill wall and sliding cracks developed along the infill-column and infill-beam interfaces as shown in Figure 9B. During the third cycle of loading, one step-type crack developed at the left of the infill wall as shown in Figure 9C, and it propagated to the right corner of the infill wall, while minor sliding cracks were also formed at the upper left and lower right corner of the infill wall. In addition, shear cracks developed at the upper ends of the columns, which were more visible at the upper end of the right column, and they propagated in the beam-column joint. During the fourth cycle of loading, the base-shear was equal to ±230 kN at a corresponding drift ratio of ±0.89%, as shown in Figure 9A, which represents a 23%−33% reduction in lateral resistance compared to that of the previous cycle. During this cycle of loading (Figures 9D,E), the previously formed step-type crack along the diagonal of the infill wall and the cracks at the upper corners of the infill wall reopened and became wider leading to the *corner crushing of the infill wall*. Furthermore, the shear cracks at the upper ends of the columns also reopened and became wider indicating the shear failure of the upper ends of the columns. Shear failure of the columns was possibly the result of a *short column mechanism* which occurred due to the partial restrain imposed by the infill wall after the failure of its upper corner part. As the displacement loading increased, a marked decrease in the lateral resistance and stiffness of the infilled frame was observed. During the last cycle of loading the base-shear was equal to 221 kN and −157 kN at corresponding displacements of 54.9 mm and −55 mm, respectively (drift ratio of ±1.96%). In this cycle, the cracking pattern was formed completely as shown in Figures 9F,G with the formation of two step-type cracks (width of the crack ranges from 5 to 10 mm) indicating

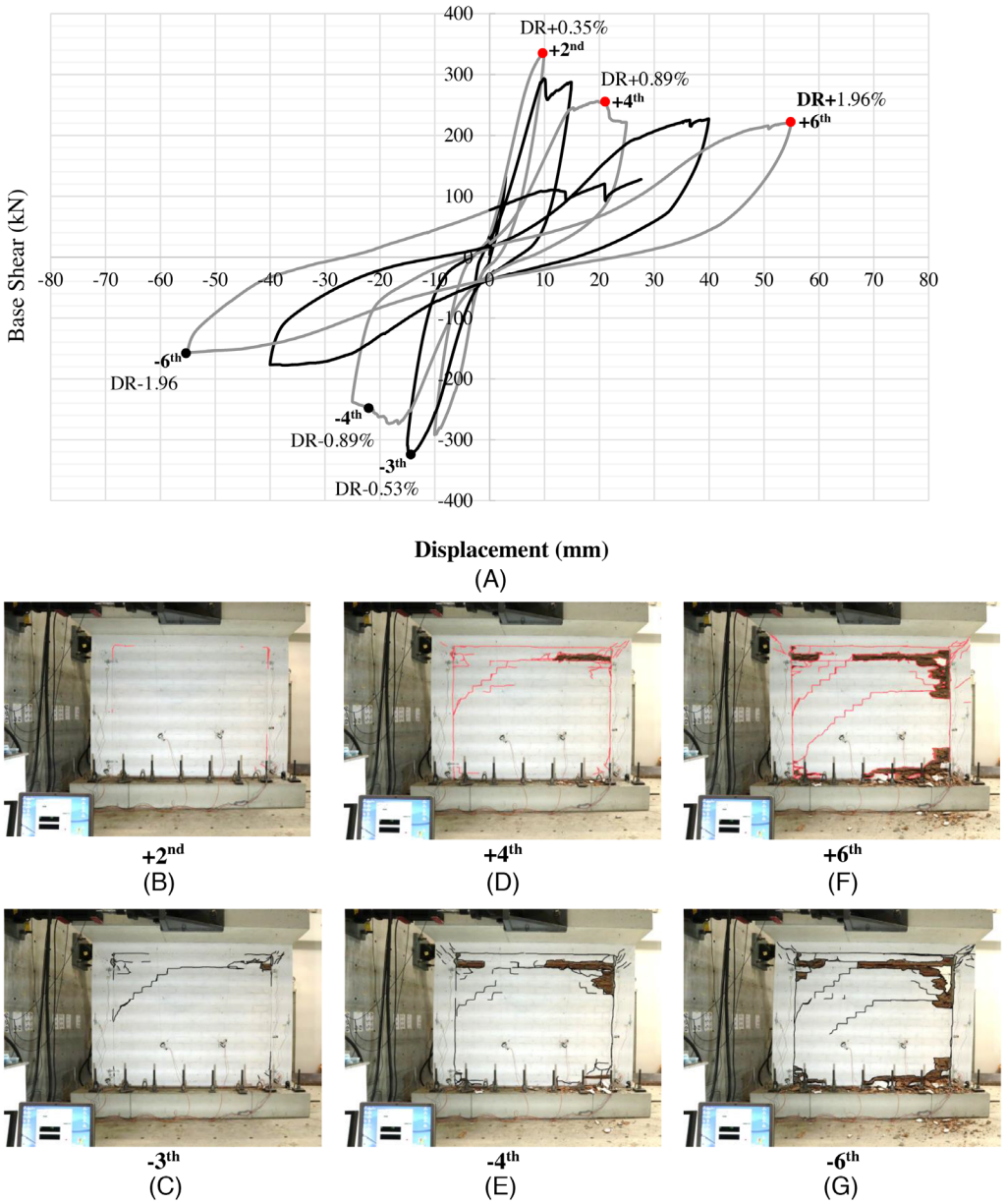

FIGURE 9 Response of M-specimen (control specimen). (A) Base-shear versus top-floor displacement, (B) the crack patterns during the second cycle of loading, (C) third cycle of loading (negative direction), (D) during the fourth cycle of loading in the positive, and (E) negative direction, and during the sixth cycle of loading (F) positive and (G) negative direction.

the *diagonal cracking* combined with *sliding shear failure* of the wall. In addition, during the last cycle of loading, *corner crushing failure* of the wall propagated, and it was more pronounced at the upper part of the infill wall than the lower part as shown in Figures 9F,G. In fact, some bricks at the upper right corner of the infill wall exhibited complete crushing with large portions of the material falling off. The ultimate failure mechanism also involved the shear failure of the upper ends of the columns (*short column mechanism*). The infill-column gap-opening measured during the last cycles of loading was in the range of 0.5–1.5 cm while the relative sliding between the infill-column interface was between 2.5–5 cm. The damage and crack pattern formed at the two sides of the specimen was practically identical.

3.2 | M-XC specimen

The M-XC specimen (Figure 1) was subjected to seven and a half cycles of displacement-controlled loading before reaching a critical damage condition. The maximum imposed displacement in this case was equal to +80 mm (+2.85% drift ratio).

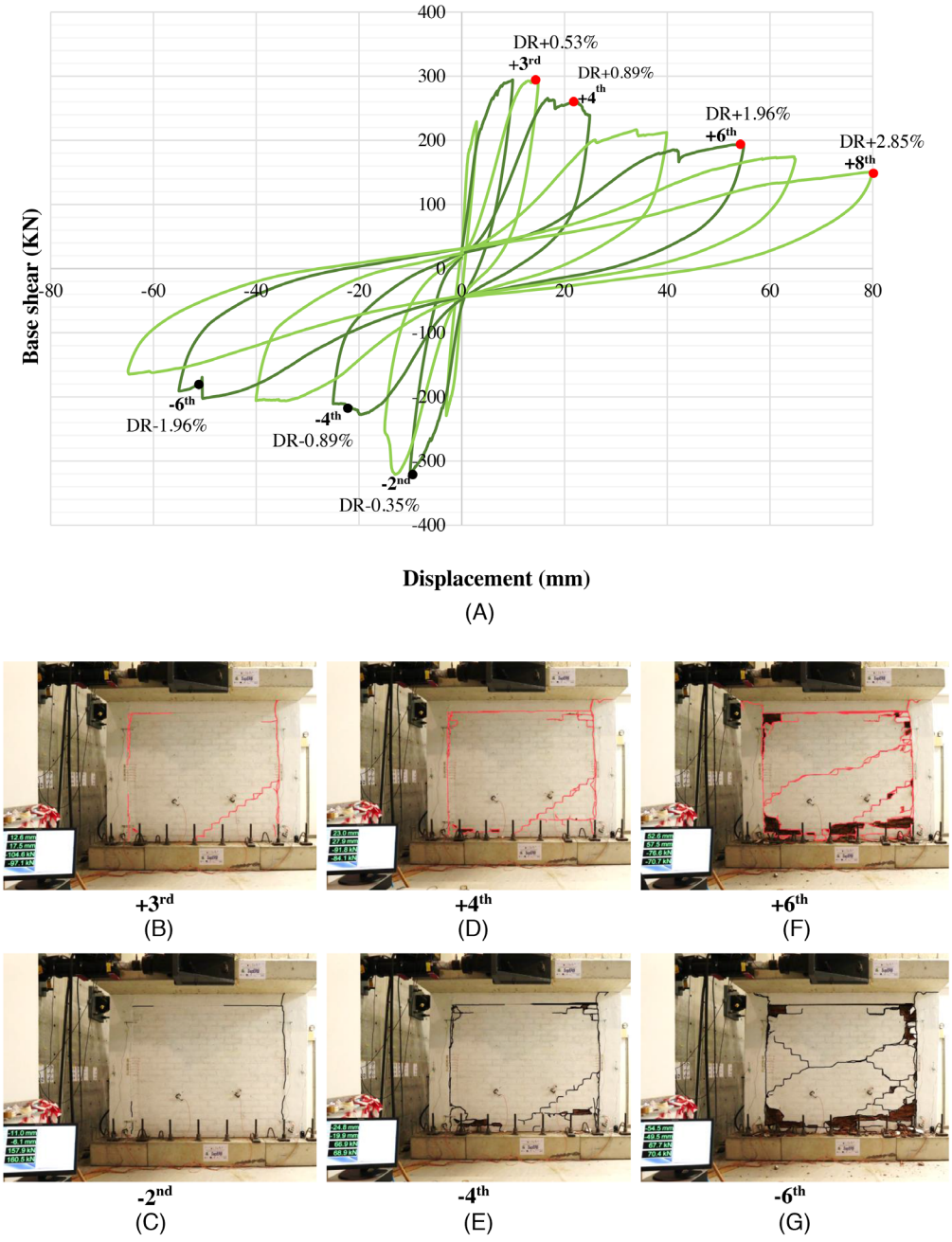

FIGURE 10 Response of M-XC specimen. (A) Base-shear versus top-floor displacement, (B) the crack patterns during the third cycle of loading, (C) second cycle of loading (negative direction), (D) during the fourth cycle of loading in the positive, and (E) negative direction, and during the sixth cycle of loading (F) positive and (G) negative direction.

Figure 10 presents the hysteresis curve and the progression of cracking at the unretrofitted side of the specimen for the second, fourth and sixth cycles of loading. In the positive direction, a maximum base-shear force equal to 296 kN was attained during the third cycle of loading when the displacement at the top of the specimen was 15 mm (drift ratio of +0.53%). In the negative direction a maximum load of −319 kN was recorded during the second cycle of loading corresponding to an imposed displacement of −10.3 mm (drift ratio of −0.35%). At the second and third cycle of loading in the positive direction, a step-type crack was formed at the lower part of the infill wall. This initiated at the mid-length of the wall's base and propagated toward the mid-height of right column as shown in Figure 10B. In addition, minor cracks developed at the lower corners of the infill wall. During the same cycles of loading, sliding cracks developed along the infill-column and infill-beam interfaces as shown in Figure 10B,C. At the fourth cycle of loading, when the imposed displacement was equal to ±25 mm (drift ratio of ±0.89%), the base-shear was equal to ±225 kN which represents a 20%−25% decrease of the lateral resistance

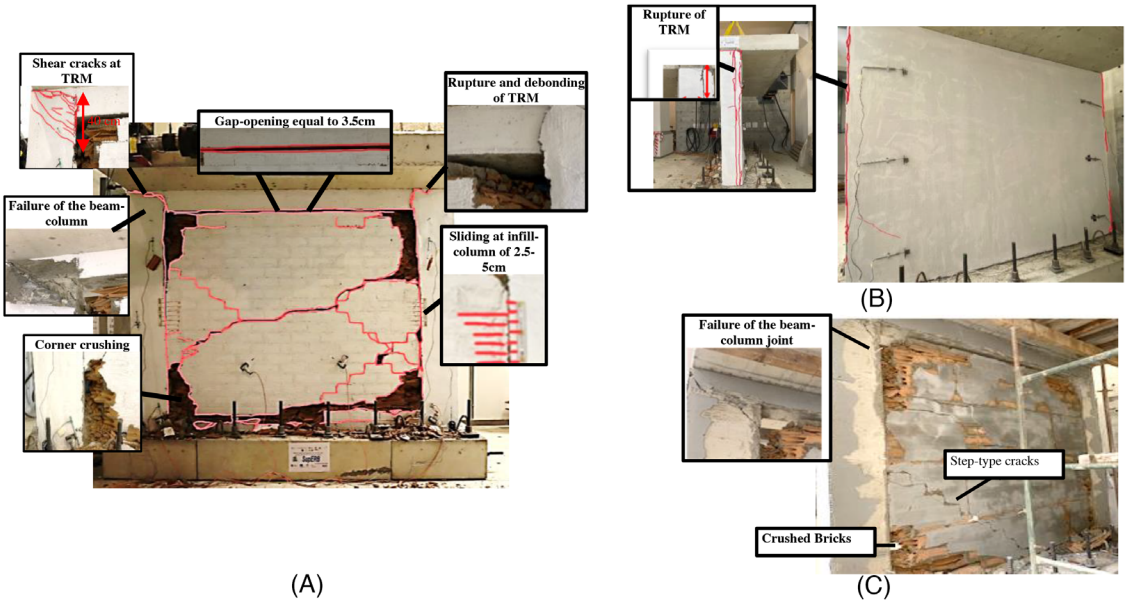

FIGURE 11 Cracking pattern and the failures occurred on M-XC specimen (A) at the unretrofitted side, (B) at the retrofitted side, and (C) after removing the retrofitting layers (XPS and TRM layer).

relative to the previous cycle. During this cycle, the previously formed step-type crack at the lower part of the infill wall and the sliding cracks at the corners of the infill wall and along the infill-frame interface reopened and became wider as shown in Figures 10D,E. As the displacement loading increased, a marked decrease in the lateral resistance and stiffness of the infilled frame was observed. In the sixth cycle of loading the base-shear was equal to ±190 kN at a corresponding drift ratio equal to ±1.96%. During this cycle, the previously formed step-type cracks and sliding cracks along the diagonal of the infill wall became wider and propagated along its entire central section indicating the *diagonal cracking* combined with *sliding shear* failure of the infill wall as shown in Figure 10F,G. In addition, during this cycle the *corner crushing failure of the wall* became more pronounced. The test was intentionally terminated at the end of the seventh and one-half cycle of loading, at a maximum displacement of approximately 80 mm (positive direction of loading) which corresponds to 2.85% drift ratio as shown in Figure 10A. The c racking pattern and the failures at the end of the test are presented in Figure 11.

Figure 11 shows the cracking patterns and the failures on both sides (retrofitted and unretrofitted sides) of the M-XC specimen after the end of the test. Figure 11A shows the rupture and debonding of the TRM, the failure of the beam-column joint indicating the *frame* failure mode (the shear cracks at the TRM at the upper end of the left column propagated diagonally to the infill wall, 40 cm from the upper end of the column), and the *corner crushing* failure of the infill wall (some bricks at the corners of the infill wall exhibited complete crushing with large portions of the materials falling off). The step-type cracks and the sliding cracks along the diagonal of the infill wall, as shown in Figure 11A, had an average crack width equal to 1−2.5 cm. The gap-opening and the sliding at the infill-column interface was about 1−2.5 and 2.5–5 cm, respectively, while the gap-opening at the upper beam-infill was about 3−5 cm as shown in Figure 11A. At the retrofitted side of the specimen no major cracks were observed on the TRM layer as it is evidenced in Figure 11B. Rupture of the TRM occurred only at the columns' corners along the height of the TRM-XPS interface. This was due to the relative slip along the TRM-XPS interface. After the completion of the test and the removal of the TRM and XPS layers, as shown in Figure 11C, it was noted that the damage and the crack patterns that occurred on the unretrofitted side of the infill wall (corner crushing, diagonal and sliding cracks, the shear cracks at the upper end of the columns, and at the beam-column joint) had propagated to the retrofitted side of the specimen. It is important to mention that the XPS board was well bonded to the infill wall surface at the end of the test. This indicates that the proposed integrated retrofitting system remained intact throughout the tests, and this prevented the fall of debris out of the plane of the infilled frame both in the retrofitted and unretrofitted sides. This is also observed for all the retrofitted specimens as will be presented in the next sections.

3.3 | M-CXC specimen

The M-CXC specimen (Figure 1) was also subjected to seven and a half cycles of displacement-controlled loading corresponding to a maximum imposed displacement of +80 mm (+1.96% drift ratio). Figure 12 presents the hysteresis curve and

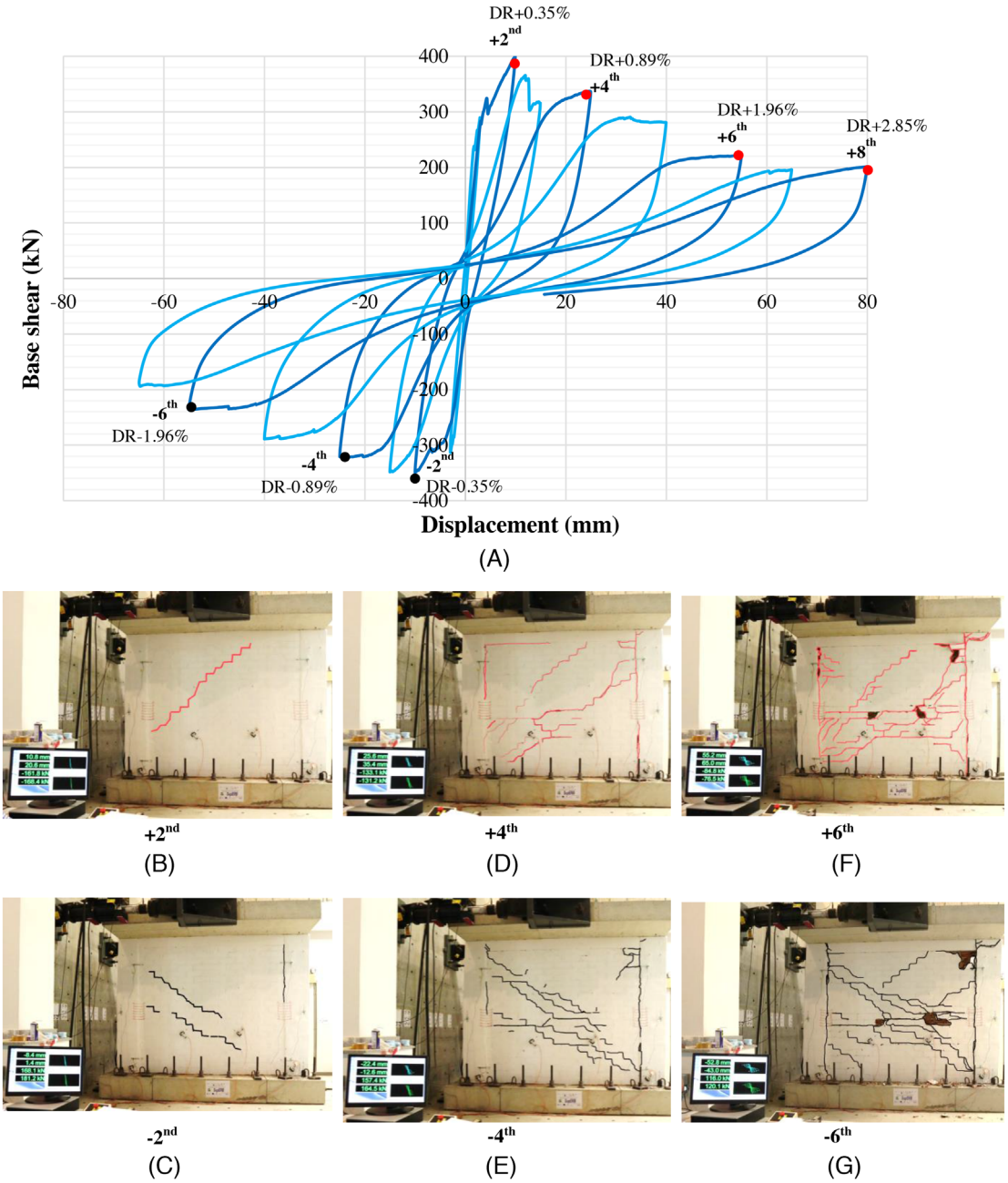

FIGURE 12 Response of M-CXC specimen. (A) Base-shear versus top-floor displacement, (B) the crack patterns during the second cycle of loading in the positive, (C) negative direction, (D) during the fourth cycle of loading in the positive, and (E) negative direction, and during the sixth cycle of loading (F) positive and (G) negative direction.

the progression of cracking at the unretrofitted side of the specimen for the second, fourth and sixth cycles of loading. The maximum base-shear force was attained during the second cycle of loading for both directions, and it was equal to 400 kN and −349 kN at corresponding top-displacements of 9.93 mm and −10.02 mm, respectively. During the second cycle of loading, step-type cracks were formed along the diagonals of the infill wall. One crack was observed when the loading was imposed in the positive direction (Figure 12B) and two cracks were observed when the loading was in the negative direction of (Figure 12C). At the same cycle of loading, minor sliding cracks also developed along the right column and the infill wall interface as indicated with black color in Figure 12C. At the third and fourth cycles of loading the base-shear force did not present a drop, unlike other specimens, and was on the average approximately ±330 kN (both in the positive and negative directions) at a corresponding top-displacement of ±15 mm (drift ratio of ±0.53%) and ±25 mm (drift ratio of ±89%), respectively. This represents an 18% decrease in the positive direction and 5% decrease in the negative one of

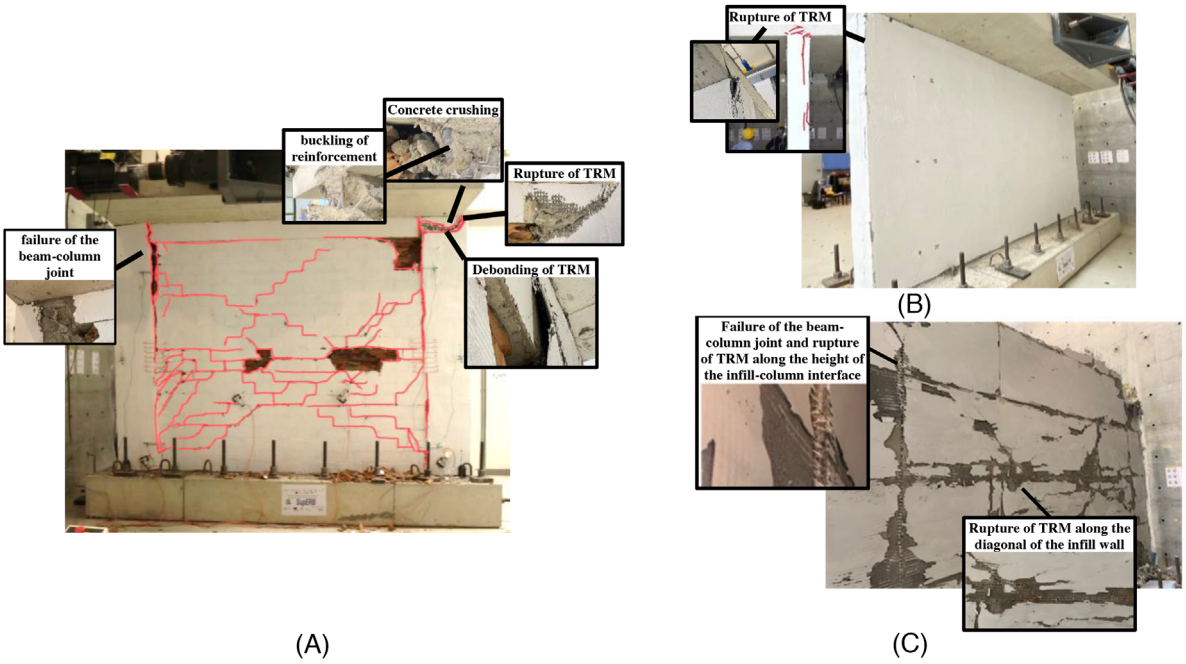

FIGURE 13 Cracking pattern and the failures occurred on M-CXC specimen (A) at the unretrofitted side, (B) at the retrofitted side, and (C) after removing the second layer of TRM and the XPS layer.

the lateral resistance relative to the corresponding ones in the second cycle of loading. During these cycles of loading, the diagonal step-type and the sliding cracks that developed on the infill wall in the previous cycle of loading became wider and propagated throughout the entire surface of the masonry infill wall (spread along the diagonal of the infill wall) as shown in Figures 12D,E. Also, sliding cracks developed along the left column-infill wall interface and propagated to the lower part of the structure, below the mid-height of the column. Furthermore, the previously formed cracks along the right column-infill wall interface reopened, became wider and propagated along the full height of the right column-infill wall interface. As the displacement loading increased, a marked decrease of the lateral resistance and stiffness of the retrofitted infilled frame was observed. By the sixth cycle of loading, when a drift of ±1.96% was reached, the lateral resistance had dropped to ±230 kN. At this cycle of loading, sliding cracks at the mid-height of the infill wall met the paths of the step-type cracks formed at previous cycles indicating the *diagonal cracking* combined with *sliding shear* failure of the infill wall. At the same time, the *corner crushing* failure became more pronounced since the bricks at the upper right corner of the infill wall exhibited crushing as shown in Figures 12F,G, while sliding cracks along the infill-column interfaces became wider indicating separation between the RC columns and the infill wall. Moreover, diagonal shear cracks that had developed during previous cycles of loading on the TRM layer covering the top-end of both RC columns became wider. This damage was more evident at the top-end of the right column and led to the rupture of the TRM at this location indicating the failure of the beam-column joint (*frame failure mode*). The test was intentionally terminated at the end of the seventh and one-half cycle of loading, at maximum-imposed displacement of approximately 80 mm (positive direction of loading) which corresponds to 2.85% drift ratio as shown in Figure 12A.

Figure 13 shows the cracking patterns and failures on both sides (retrofitted and unretrofitted sides) of the M-CXC specimen after the end of the test. Figure 13A shows the *corner crushing* of the infill wall, the step-type cracks, and the sliding cracks along the diagonal of the infill wall (*diagonal cracking failure mode combined with sliding shear failure mode of the infill wall*). Figure 13A shows the debonding of TRM from the upper ends of both columns and the rupture of the textile reinforcement at the upper end of the right column. After the completion of the test and the removal of the retrofitting layers, as shown in Figure 13A, it was observed that the underlying concrete at the upper end of the right column had suffered extensive spalling. This indicates failure of the beam-column joint (*frame failure mode*). At this area, the textile reinforcement of the first layer of TRM ruptured, while buckling of the longitudinal steel reinforcement also occurred. Debonding and rupture of the TRM was observed only at the upper ends of columns (near the beam-column joint) during the last cycles of loading. At the retrofitted side of the specimen, no major cracks were observed on the exterior surface of the second TRM layer as evidence by Figure 13B. However, rupture of the textile embedded in the TRM

was observed at the columns' corners along the height of the TRM-XPS interface as shown in Figure 13B. This was due to the relative slip along the TRM-XPS interface and to the shear failure of the columns. After the completion of the test and the removal of the second layer of TRM and the XPS layer, as shown in Figure 13C, it was noted that that rupture of the first layer of TRM had also occurred along the perimeter of the column-infill interface and at the mid-height of the infill wall. In the latter case, rupture was recorded a height of 1.1 m from the base and extended horizontally along the length of the specimen, which coincides with the location where the step-type and sliding cracks developed on the unretrofitted side of the infill wall. After removal of all retrofitting layers, it was observed that the step-type cracks along the diagonal of the infill wall and the shear cracks at the upper end of the columns (near the beam-column joint), which had been developed on the unretrofitted side of the specimen, had also propagated to the other side of the specimen.

3.4 | M-P specimen

The M-P specimen (Figure 1) was subjected to six cycles of loading before reaching a critical damage condition. The maximum imposed displacement in this case was equal to ±55 mm (±1.96% top drift ratio). It is important to mention that soon after the completion of the retrofitting layer, comprising of glass textile reinforcement (Table 1) and of PCM-enhanced mortar, minor shrinkage cracks developed on the retrofitting side of the specimen. Although most of these cracks were hairline, their presence may have influenced the effectiveness of the TRM retrofitting technique. Figure 14 presents the hysteresis curve and the progression of cracking at the unretrofitted side of the specimen for the second, fourth and sixth cycles of loading. In the positive direction, the maximum base-shear force was equal to +284 kN and was attained during the second cycle of loading when the top-displacement was +9.9 mm (drift ratio of +0.35%). In the negative direction, a maximum base-shear force of −312 kN was recorded during the third cycle of loading when the top-displacement was −15 mm (drift ratio of −0.53%). During the second cycle of loading, in the positive direction, one step-type crack was formed along the diagonal of the infill wall (Figure 14B). This step-type crack reopened and became wider in third cycle of loading. The crack formed at this cycle of loading was accompanied by the formation of sliding cracks at the lower corners of the infill wall and along the infill-column and infill-beam interfaces (Figure 14C). During the fourth cycle of loading, the base-shear was equal to ±224 kN at a corresponding drift ratio of ±0.89%. This represents an 22% decrease in the positive direction relative to the corresponding one in the second cycle of loading, and 28% decrease in the negative one of the lateral resistance relative to the corresponding one in the third cycle of loading. At this cycle of loading, the diagonal step-type that had developed on the infill wall became wider and propagated toward the right corner of the infill wall. In addition, minor sliding cracks were also formed at the upper right and lower left corner of the infill wall (Figure 14D,E). During the fifth cycle of loading at a corresponding drift ratio equal to ±1.43% the shear and sliding cracks near the corners of the infill wall reopened and became wider resulting to the *corner crushing failure* of the infill wall. As the imposed displacement increased, a marked decrease in the lateral resistance and stiffness of the infilled frame was observed. By the last cycle of loading the lateral resistance dropped to +190 kN and −150 kN at a corresponding displacement of 54.9 mm and −55 mm, respectively (drift ratio of ±1.96%). At this cycle of loading, the step-type crack along the diagonal of the infill wall became wider indicating the *diagonal cracking* failure mode combined with *sliding shear* failure mode of the infill wall, while the wall's corners exhibited complete crushing (Figure 14F,G). The final cracking pattern also included sliding cracks along the infill-column interfaces indicating separation and relative sliding between the RC columns and the infill wall. Finally, shear cracks were observed on the TRM layer covering the top-end of both RC columns indicating the failure of the beam-column joint (*frame failure mode*).

Figure 15 shows the cracking patterns and failures on both sides (retrofitted and unretrofitted sides) of the M-P specimen after the end of the test. Figure 15A shows the *corner crushing* of the infill wall (the bricks at the upper corners of the infill wall exhibited almost complete crushing), and the failure of the beam-column joints (the crack width at the upper end of the column was equal to 4−5 mm near the beam-column joint, and 2−3 mm near the infill-frame interface). Figure 15A shows the debonding of TRM from the upper ends of both columns. At the retrofitted side of the specimen cracks developed at the TRM retrofitting layer along the perimeter of the frame-infill interface. Nevertheless, rupture of TRM occurred only along the height of the columns' corners where the retrofitting layer was wrapped around the RC frame (Figure 15B). After the completion of the test and the removal of the retrofitting layers, as shown in Figure 15C, revealed that the shear cracks observed on the un-retrofitted side at the upper ends of the columns (near the beam-column joint) had propagated to the back side of the specimen. This verifies the occurrence of brittle failure at the beam-column joints (*frame failure mode*). Furthermore, some bricks at the upper corner of the infill wall exhibited complete crushing, likewise to what was observed on the unretrofitted side of the specimen. It is important to mention that the TRM with PCMs layer was well

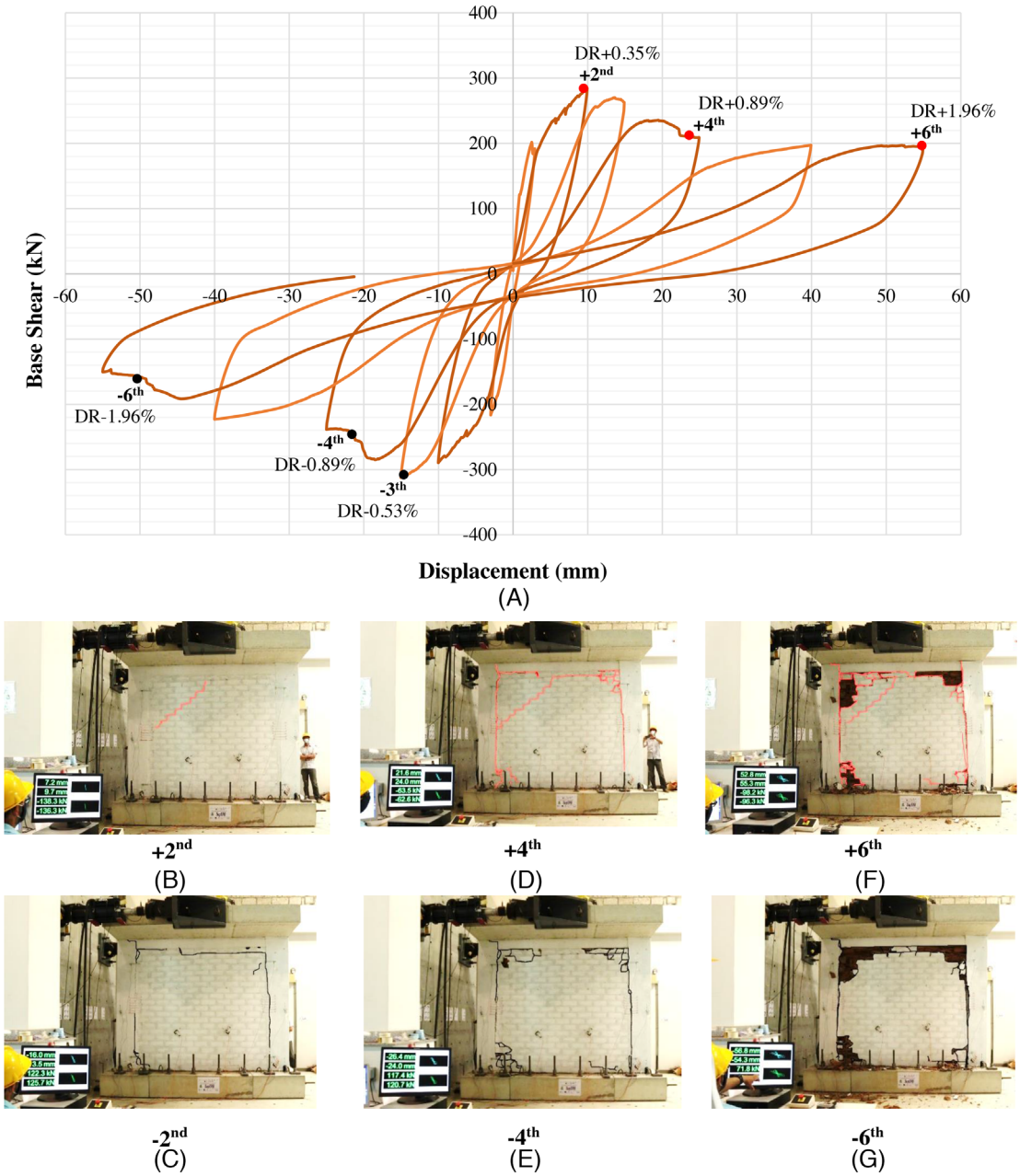

FIGURE 14 Response of M-P specimen. (A) Base-shear versus top-floor displacement, (B) the crack patterns during the second cycle of loading in the positive, (C) in the negative direction, (D) during the fourth cycle of loading in the positive, and (E) negative direction, and during the sixth cycle of loading (F) positive and (G) negative direction.

bonded to the infill wall. In fact, during the removal of the retrofitting fragments of the masonry substrate would remain attached to the overlay (Figure 15C).

3.5 | M-CXP specimen

The M-CXP (Figure 1) specimen was subjected to the full eight cycles of loading history which resulted to a maximum imposed displacement of ±80 mm (±2.85% drift ratio). Figure 16 presents the hysteresis curve and the progression of cracking at the unretrofitted side of the specimen for the second, fourth and sixth cycles of loading. The maximum base-shear force was attained during the second cycle of loading for both directions equal to 353 kN and −339 kN at corresponding top-displacement of 9.9 mm and −10 mm, respectively. During the second cycle of loading in the positive direction,

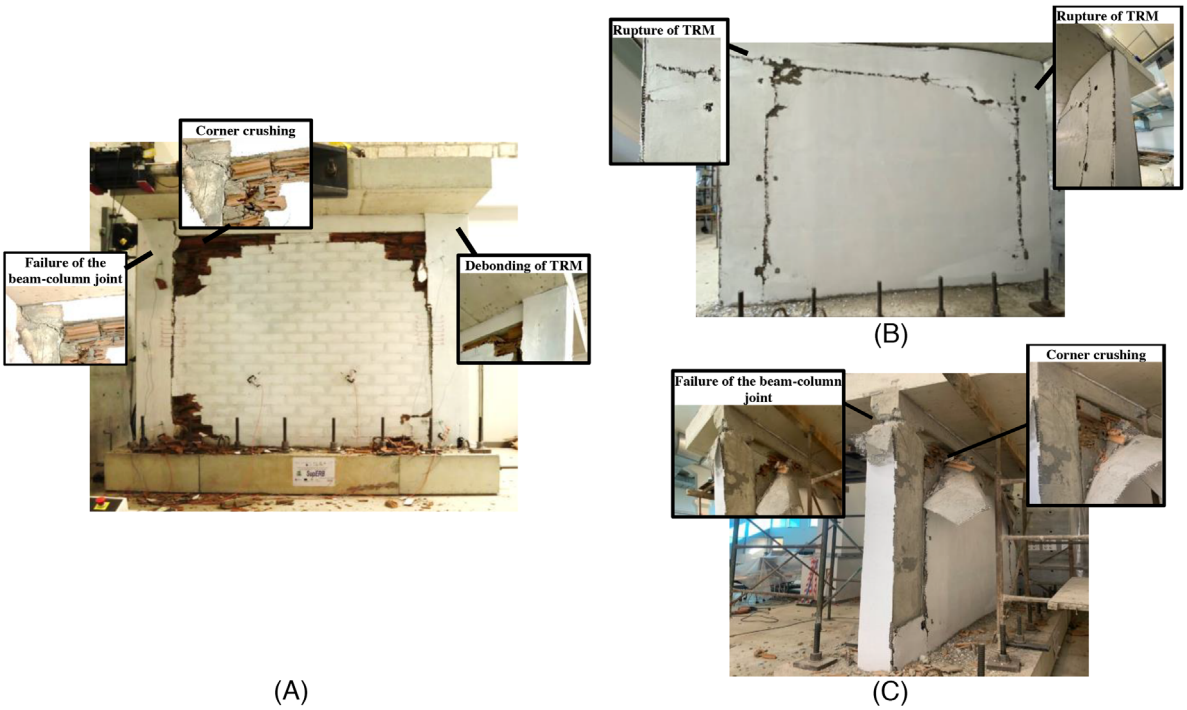

FIGURE 15 Cracking pattern and the failures occurred on M-P specimen (A) at the unretrofitted side, (B) at the retrofitted side, and (C) after removing the TRM retrofitting layer.

one step-type crack was formed along the diagonal of the infill wall. This crack initiated at the left-side and propagated rapidly to the right-side of the infill wall (Figure 16B). In the negative direction of loading a similar step-type crack was formed starting from the right-side to the left-side of the infill. During this cycle of loading minor sliding cracks also developed along the right column-infill wall interface and along the infill-beam interface as indicated with black color in Figure 16C. At the third and fourth cycles of loading the base-shear did not present a drop, unlike other specimens, and was on the average approximately ±320 kN (both in the positive and negative directions) at a corresponding top-displacement of ±15 mm (drift ratio of ±0.53%) and ±25 mm (drift ratio of ±89%), respectively. This represents a 5%–10% decrease of the lateral resistance relative to that of the second cycle of loading. During these cycles of loading, the step-type and horizontal sliding cracks that had developed along the diagonal of the infill wall propagated to the entire body of the wall as shown in Figures 16D,E. Also, shear cracks were formed at the second layer of TRM (in which PCM-enhanced mortar was used) that covers the top-ends of the two RC columns. At the same time, the previously formed sliding cracks at the right column-infill wall interface (upper side of the column), reopened, became wider and propagated along the full height of the right column. As the displacement loading increased, a marked decrease of the lateral resistance and stiffness of the retrofitted infilled frame was observed. At the sixth cycle of loading the base-shear was equal to ±262 kN at the corresponding drift ratio equal to ±1.96%. At this cycle of loading, the sliding cracks at the mid-height of the infill wall met the paths of the step-type cracks formed at previous cycles indicating the *diagonal cracking* failure mode combined with *sliding shear* failure mode of the infill wall, while the bricks at the upper right corner of the infill wall were completely crashed indicating the *corner crushing failure* of the infill wall as shown in Figures 16F,G. Also, the diagonal shear cracks that had opened in previous cycles at the second layer of TRM with PCMs overlaying the top-ends of both columns (near the beam-column joint) became wider, especially at the top-end of the right column. This led to rupture of the retrofitting layer at this location indicating the failure of the beam-column joint (*frame failure mode*). The test was intentionally terminated at the end of the eighth cycle of loading, at a maximum-imposed displacement of approximately ±80 mm which corresponds to ±2.85% drift ratio as shown in Figure 16A.

Figure 17 shows the cracking patterns and the failures on both sides (retrofitted and unretrofitted side) of the M-CXP specimen after the end of the test. Figure 17A shows the *corner crushing* of the infill wall, the step-type cracks and the sliding cracks along the diagonal of the infill wall (*diagonal cracking failure mode combined with sliding shear failure mode of the infill wall*). Figure 17A also presents the debonding of the TRM from the upper ends of both columns and the rupture of the textile reinforcement at the upper ends of the columns. At the end of the test and after the removal of the retrofitting

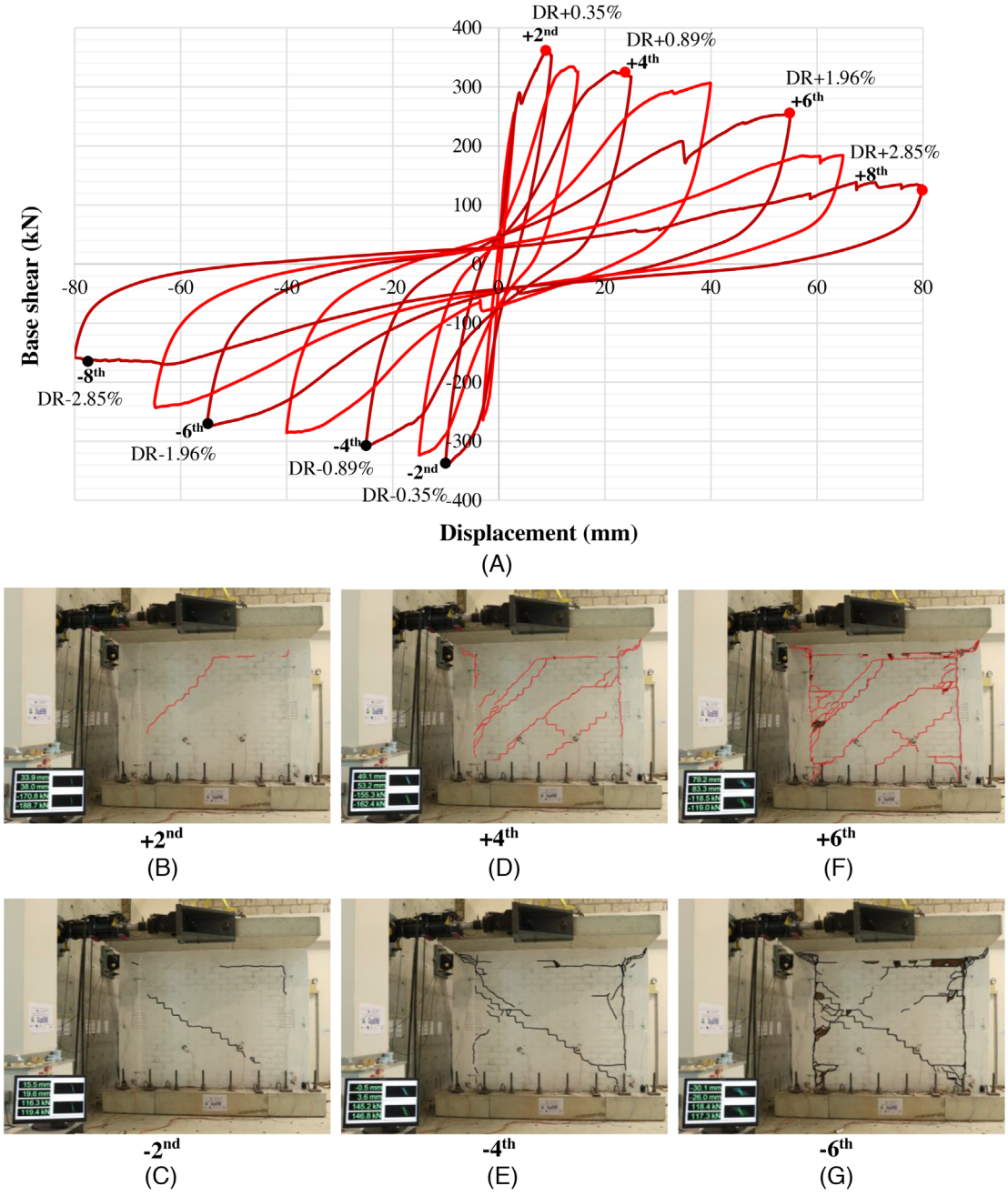

FIGURE 16 Response of M-CXP specimen. (A) Base-shear versus top-floor displacement, (B) the crack patterns during the second cycle of loading in the positive, (C) negative direction, (D) during the fourth cycle of loading in the positive, and (E) negative direction, and during the sixth cycle of loading (F) positive and (G) negative direction.

layers it was observed that at the upper end of the columns, the concrete suffered severe damage indicating the failure of the beam-column joint (*frame failure* mode). Therefore, at a high drift ratio, the TRM cannot successfully prevent the brittle failure of the beam-column joint, but it should be underlined that it is delayed to a displacement which is 50% larger than that of the control specimen. Nevertheless, if such large displacements are expected, and taking into consideration the joint weakness of existing frames, beam-column joints may need to be strengthened. At this area, the textile reinforcement of the first TRM layer was ruptured, while buckling of the longitudinal steel reinforcement also occurred. Thus, the M-CXP specimen exhibited significant residual deformation at the end of the test. A permanent deformation of 10 cm was measured, since the initial length of the specimen was equal to 3.60 m and the length of the specimen along the damaged upper ends of the columns was equal to 3.70 m at the end of the test (Figure 17A). At the retrofitted side of the specimen no major cracks were observed on the exterior (second layer) TRM retrofitting layer (TRM with PCMs). However, rupture

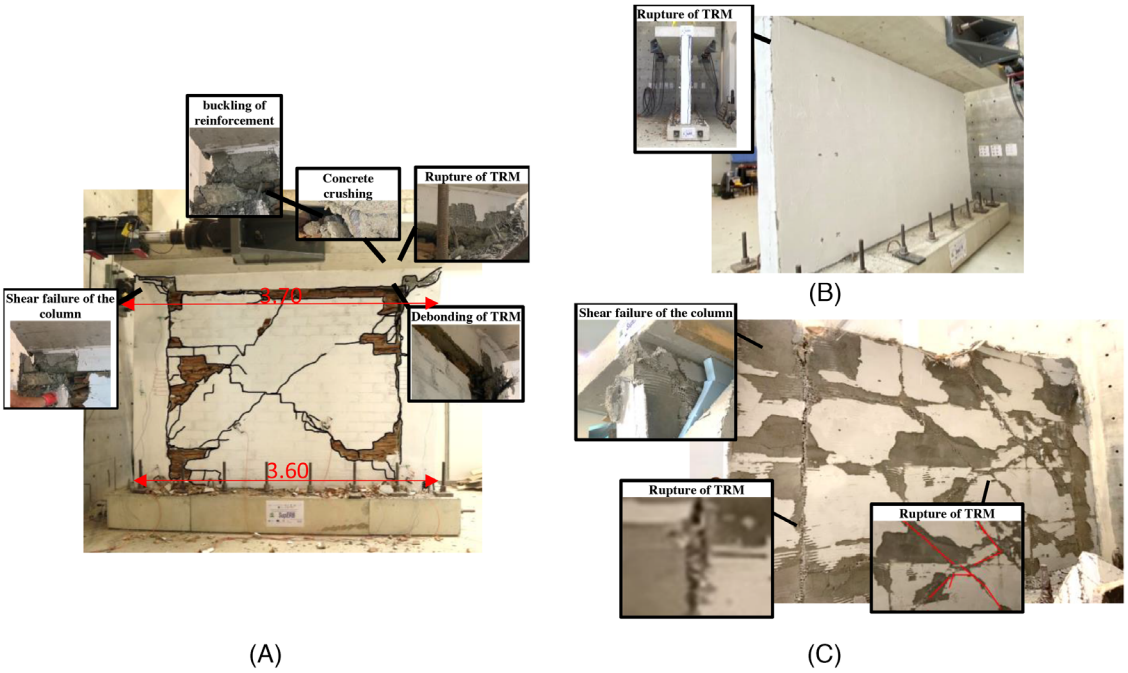

FIGURE 17 Cracking pattern and the failures occurred on M-CXP specimen (A) at the un-retrofitted side, (B) at the retrofitted side, and (C) after removing the second layer TRM (in the second layer of TRM with PCM).

of the textile reinforcement was observed at the columns' corners along the height of the interfaces between the XPS and the first and second layers of TRM (Figure 17B). The brittle rupture of TRM may again be attributed to the relative slip between the TRM and the XPS and due to the shear failure of the columns. After removal of the exterior TRM layer and the XPS board (Figure 17C), it was observed that rupture of the first TRM layer had occurred along the column-infill interface, along the diagonal of the infill wall and horizontally along the mid-height of the specimen. The diagonal and horizontal cracks at the first TRM layer coincided with the locations where the step-type and sliding cracks developed in the un-retrofitted side of the specimen. It was also observed that rupture of the TRM occurred at the columns' corners along the height of the TRM-XPS interface. Large shear and tensile cracks developed also on the first layer of TRM. These initiated from the exterior edges of the columns and propagated toward the corners that were in contact with the compression diagonal of the infill wall, thus leading to failure of the beam-column joint. It is important to mention that after the completion of the test the first layer of TRM remained fully bonded to the infill wall, despite the rupture of the textile.

4 | COMPARISON OF THE RESULTS

In this section, the results obtained from the testing of the five masonry-infilled RC frame specimens and presented in the previous section are compared, aiming to assess the in-plane lateral performance of the masonry-infilled RC frames retrofitted with different schemes of TRM combined with thermal insulation materials that were examined in this study. Table 4 provides comparison of the specimens' global and local behavior (cracking patterns and failures), summarizing the information given in the previous sections.

Figure 18 compares the envelopes of the base shear versus drift ratio curves until the third cycle of loading, which corresponds to 0.53% drift ratio (Figure 18A), and up to the total duration of the test (Figure 18B). Table 3 gives the peak base-shear ($V_{\max,+ve}$ and $V_{max,-ve}V_{\max,-ve}$) and the peak drift ratio ($DR_{\max,+ve}$ and $DR_{\max,-ve}$) in the positive and negative directions of loading.

From Figure 18A it is observed that up to about a drift ratio of +0.2% or −0.3% in the negative direction the lateral resistance of the retrofitted infilled frames is higher than that of the control specimen (black line in Figure 18A), regardless of the retrofitting scheme. Moreover, a substantial increase is observed in the initial lateral stiffness that is calculated from the base-shear—displacement data of the first loading cycle (up to a drift ratio of ±0.1%); see also Figure 20A. In all cases, the maximum base-shear force was attained during the second or third cycle of loading which corresponds to 0.35%–0.53%

TABLE 3 Summary of the peak base-shear and the peak drift ratio in each cycle of loading; for the two directions of loading, $V_{max,+ve}$ and $DR_{max,+ve}$ (positive direction of i^{th} cycle) and $V_{max,-ve}$ and $DR_{max,-ve}$ (negative direction of i^{th} cycle).

Number of cycles	Drift ratio * $DR_{max,\pm ve}$	M-Control specimen		M-XC specimen		M-CXC specimen		M-P specimen		M-CXP specimen	
Positive	Negative	Positive	Negative	Positive	Negative	Positive	Negative	Positive	Negative		
$V_{max,+ve}$	$V_{max,-ve}$	$V_{max,+ve}$	$V_{max,-ve}$	$V_{max,+ve}$	$V_{max,-ve}$	$V_{max,+ve}$	$V_{max,-ve}$	$V_{max,+ve}$	$V_{max,-ve}$		
1st	±0.10%	131.73	−79.62	229.02	−229.32	289.42	−312.59	191.69	−216.32	255.82	−263.83
2nd	±0.35%	335.03	−291.56	294.22	−318.65	400.76	−349.45	284.55	−289.53	353.11	−339.02
3rd	±0.53%	287.29	−309.23	295.82	−252.01	315.97	−348.25	262.77	−312.52	325.47	−323.23
4th	±0.89%	221.33	−237.54	239.16	−210.75	336.04	−320.86	209.08	−238.60	317.22	−308.27
5th	±1.43%	227.01	−176.80	212.37	−205.92	280.89	−288.96	197.37	−222.94	306.30	−285.66
6th	±1.96%	220.58	−157.24	193.87	−190.94	222.19	−236.47	190.01	−150.21	251.70	−273.81
7th	±2.32%			170.96	−158.53	196.06	−185.39			184.19	−232.92
8th	±2.85%			150.83		201.54				132.87	−158.72

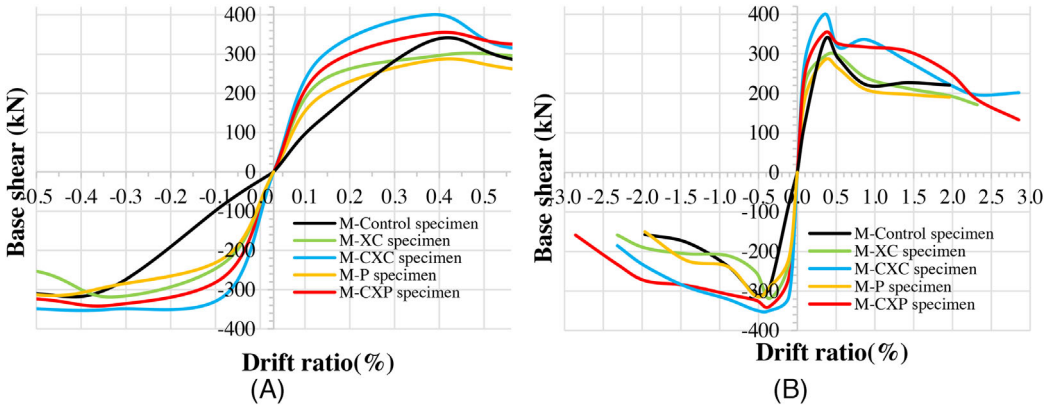

FIGURE 18 Envelopes curves for all specimens in terms of base-shear versus drift ratio (A) until the third cycle of loading at the corresponding drift ratio of 0.53% and (B) total duration of the test.

drift ratio. Further comparison of the various schemes used is presented in Table 4. From Figure 18B it is observed that the drift ratio of the specimens retrofitted with two layers of TRM with or without PCMs is equal to 2.85%, which corresponds to a displacement capacity of +80 mm, while for the un-retrofitted specimen (M-control specimen, black line) it is equal to ±1.96% drift ratio (±55 mm displacement capacity). Thus, the displacement capacity of infilled frames increases by 45% by using two layers of TRM with or without PCMs. It can be also observed that the response of the infilled frame retrofitted with a single layer of TRM with PCM (M-P specimen, yellow line) is almost the same with the unretrofitted one (M-control specimen, black line) after the 0.35%–0.53% drift ratio.

Figure 18B shows that after exceeding a 0.53% drift ratio, the lateral resistance of the infilled frames retrofitted with two layers of TRM (M-CXC and M-CXP specimen, blue and red line, respectively) increases compared to that of the un-retrofitted one (M-control specimen black line) and compared to that of the infilled frames retrofitted either with one layer of TRM or one layer of TRM with PCMs (M-XC and M-P specimen, green and yellow line, respectively). The increased strength is maintained for large levels of imposed displacement. This is also supported by Figure 19 which shows the decrease of the maximum base-shear of each specimen in relation to the drift ratio. In this figure the maximum base-shear of each specimen is also presented in a tabular form. The dotted black line indicates the 20% decrease in the maximum strength. Looking in the negative direction of loading it is observed that the control specimen reaches the 20% mark (corresponding to 247 kN lateral strength) at a drift of about 0.75%. At that point the reduction in the lateral resistance of specimens M-CXC and M-CXP is about 7% (corresponding to a lateral strength of 325 and 315 kN, respectively). The M-CXC specimen reaches the 20% limit at a drift of about 1.5% and exhibits a lateral resistance of 280 kN at this stage which is 13% higher than the respective residual strength of the control specimen. At the same drift level, the control specimen suffered 43% reduction in strength and its capacity fell to 176 kN which is 37% lower than M-CXC. The 20% drop

TABLE 4 Comparison of the specimens tested in this experimental program.

Comparison	Global behavior	Local behavior failures
M-XC specimen vs. M-control specimen	1. The base-shear of M-XC specimen is increased compared to that of the control one by about (a) 74%−188% at the first cycle of loading (<0.12% drift ratio) (b) 3% at the maximum base shear at the drift ratio of 0.35%–0.53% and (c) 5% after the maximum base shear is reached (from 0.53% to 1.96% drift ratio). 2. The displacement capacity of M-XC is equal to +80 mm (2.85%-drift ratio) while for M-control specimen is equal ±55 mm (±1.96% drift ratio). 3. The secant stiffness and the dissipated energy is almost the same for the two specimens except for the first cycle of loading where the stiffness and the dissipated energy of the M-XC specimen is by 117% and 74% respectively compared to that of the control one.	1. The crack patterns and the failures that occurred on both specimens are almost the same, but they occurred in different cycles of loading. 2. The width of the cracks in the M-specimen is larger than that of M-XC one 3. The shear failure of the upper ends of the columns (short column mechanism) was not observed in the M-XC specimen (beam-column joint failure occurred) and the corner crushing of the infill wall are more pronounced in M-specimen compared to M-XC one.
M-CXC specimen vs. M-XC specimen	1. The base-shear of the M-CXC specimen is increased compared to that of the M-XC one by about (a) 26%−36% at the first cycle of loading (<0.12% drift ratio) (b) 10%−36% at the maximum base shear at the drift ratio of 0.35% and (c) 7%−52% after the maximum base shear is reached (from 0.35% to 2.85% drift ratio). 2. The displacement capacity for both specimens is the same equal to 80 mm (2.85%-drift ratio). 3. The secant stiffness and the dissipated energy of the M-CXC specimen is increased by 16%−46% by 18%−35%, respectively compared to that of the M-XC one.	• The failures that occurred on both specimens are almost the same, but they occurred in different cycles of loading • The crack patterns are more widely spread over the infill wall in the M-CXC specimen compared to those of the M-XC one • The failure of the beam-column joints (frame failure mode) and the corner crushing of the infill wall are more pronounced in the M-XC specimen compared to the M-CXC one
M-CXC specimen vs. M-control specimen	• The base-shear of the M-CXC specimen is increased compared to that of the control one by about (a) 120%−293% at the first cycle of loading (<0.12% drift ratio) (b) 20% at the maximum base shear at the drift ratio of 0.35% and (c) 10%−63% after the maximum base shear is reached (from 0.35% to 1.96% drift ratio). • The displacement capacity of the M-CXC specimen is equal to 80 mm (2.85%-drift ratio) while for the M-control specimen is equal ±55 (±1.96%-drift ratio). • The secant stiffness and the dissipated energy of the M-CXC specimen is increased by 11%−43% and 26%−46% respectively compared to that of the M-control specimen, except from the initial stiffness and dissipated energy which is increased by 185% and 120%, respectively, compared to that of the control one.	• -The crack patterns and the failures that occurred on the M-control specimen are more brittle and localized compared to that occurred on the M-CXC one • -The shear failure of the upper ends of the columns (short column mechanism) was not observed in the M-CXC specimen (beam-column joint failure occurred) and the corner crushing of the infill wall are more pronounced in M-specimen compared to the M-CXC one.
M-P specimen vs. M-control specimen	• -The base-shear of the M-P specimen during the first cycle of loading (which corresponds at 0.12% drift ratio) in the positive direction is increased by 46% compared to that of the control one. • -The maximum base-shear of the M-P specimen is attained during the third cycle of loading at the corresponding drift ratio of 0.53% while the maximum base-shear of the control specimen is attained during the second cycle of loading in the positive direction (at the 0.35% drift ratio) and during the third cycle of loading in the negative direction. The maximum base-shear for the two specimens is almost the same. • -The secant stiffness and the dissipated energy is almost the same for the two specimens except for the first cycle of loading where the stiffness and dissipated energy of the M-P specimen is increased by 93% and by 46% respectively compared to that of the M-control one	1. The crack patterns and the failures that occurred on both specimens are almost the same, but they occurred in different cycles of loading. 2. The width of the cracks in the M-control specimen is larger than that of the M-T+PCM1 one 3. The gap-opening along the infill-frame interface is wider in the M-control specimen than in the M-T+PCM1 one 4. The shear failure of the upper ends of the columns (short column mechanism) was not observed in the M-T+PCM1 specimen (beam-column joint failure occurred) and the corner crushing of the infill wall are more pronounced in the M-specimen compared to the M-T+PCM1 one.

(Continues)

TABLE 4 (Continued)

Comparison	Global behavior	Local behavior failures
M-XC specimen vs. M-P specimen	1. The maximum base-shear for both specimens occurred during the second cycle of loading at the corresponding drift ratio of 0.35% 2. The base-shear of the M-XC specimen is increased compared to that of the M-P one by about (a) 6%−19% at the first cycle of loading (<0.12% drift ratio) (b) 10% at the maximum base shear at the drift ratio of 0.35% and (c) 8%−27% after the maximum base shear is reached (from 0.35% to 1.96% drift ratio). 3. The displacement capacity of M-XC specimen is equal to 2.85% drift ratio while for M-P one is equal ±1.96%. 4. The secant stiffness and the dissipated energy is almost the same for the two specimens except for the first cycle of loading where the stiffness and the dissipated energy of the M-XC specimen is increased by 12% and 19%, respectively, compared to that of the M-P one.	1. The crack patterns are more widely spread over the infill wall in the M-XC specimen compared to those of the M-P one 2. The width of the cracks in the M-XC specimen is smaller than that of the M-P one 3. The failure of the beam-column joint (frame failure mode) and the corner crushing of the infill wall are more pronounced in the M-P specimen compared to M-XC one.
M-CXC specimen vs. M-CXP specimen	I. The base-shear of the M-CXC specimen is increased compared to that of the M-CXP one by about (a) 13%−18% at the first cycle of loading (<0.12% drift ratio) (b) 3%−13% at the maximum base shear at the drift ratio of 0.35% II. The displacement capacity for both specimens is the same equal to 2.85% drift ratio. III. The secant stiffness and the dissipated energy almost the same for the two specimens except at the first cycle of loading where the secant stiffness and the dissipated energy of the M-CXC specimen is increased by 16% and 13% compared to that of the M-CXP one.	1. The crack patterns and the failures that occurred on both specimens are almost the same 2. The crack patterns are more spread and less localized over the infill wall in M-CXC specimen compared to the M-CXP one 3. The failure of beam-column joints (*frame failure mode*) and the corner crushing of the infill wall are more pronounced in M-CXC specimen compared to M-CXP one.
M-CXP specimen vs. M-control specimen	1. The base-shear of the M-CXP specimen is increased compared to that of the control one by about (a) 94%−231% at the first cycle of loading (<0.12% drift ratio) (b) 5%−16% at the maximum base shear at the drift ratio of 0.35% and (c) 13%−74% after the maximum base shear is reached (from 0.35% to 1.96% drift ratio). 2. The displacement capacity of M-CXP specimen is equal to 80 mm (2.85%-drift ratio) while for the M-control one is equal ±55 (±1.96%-drift ratio). 3. The secant stiffness and dissipated energy of the M-CXP specimen is increased by 11%−39% and by 19%−28%, respectively, compared to that of control one except from the first cycle of loading where this increase is equal to 146% for the secant stiffness and 94% for the dissipated energy.	1. The crack patterns and the failures that occurred on M-control specimen are more brittle and localized compared to those that occurred on M-CXP specimen. 2. The shear failure of the upper ends of the columns (short column mechanism) was not observed in the M-T1-P-T+PCM2 specimen (beam-column joint failure occurred) and the corner crushing of the infill wall are more pronounced in M-specimen compared to M-CXP one.

in capacity for specimen M-CXP is reached at a drift of 2%, corresponding to 271 kN lateral strength which is 10% higher than that of the residual strength of the control specimen. At 2% drift the reduction of strength of the control specimen is about 50% and corresponds to a lateral resistance of 155 kN lateral strength which is 43% lower than that of M-CXP. The comparison of the response of each specimen tested in this experimental program in terms of strength and displacement capacity using the data presented in Table 3 is summarized in Table 4.

Figure 20 shows the global secant stiffness in relation to the number of cycles of loading and the secant stiffness after the second cycle of loading (after the 0.35% drift ratio) in relation to the number of cycles of loading. The secant stiffness degradation at the i^{th} cycle is calculated as follows (Equation (1)):

$$K_i = \frac{\left|+V_{\max,+\text{ve}}\right| + \left|-V_{\max,-\text{ve}}\right|}{\left|+X_{\max,+\text{ve}}\right| + \left|-X_{\max,-\text{ve}}\right|} \tag{1}$$

where $|+V_{max,+ve}|$ is the absolute value of the positive peak base-shear value of the i^{th} cycle as presented in Table 3, and $|+X_{\max,+\text{ve}}|$ is the absolute value of displacement corresponding to the positive peak base-shear of the of i^{th} cycle.

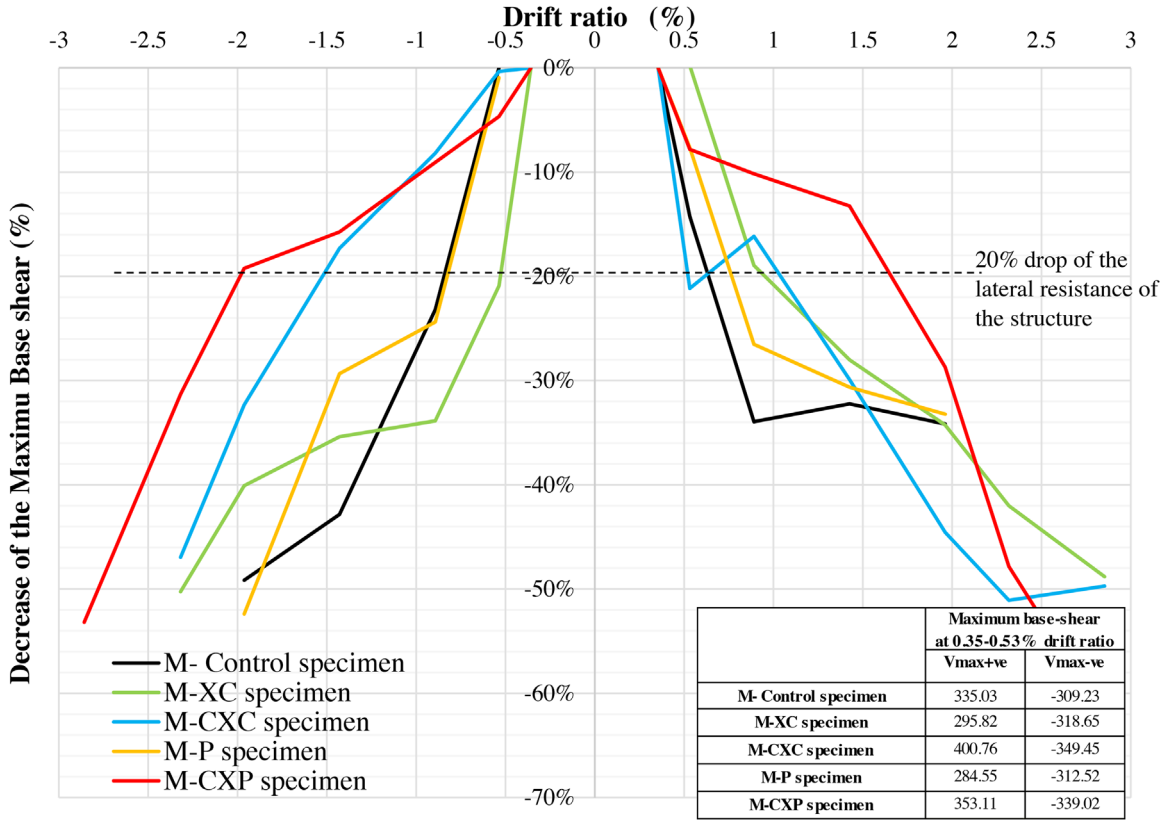

	Maximum base-shear at 0.35-0.53% drift ratio	
	Vmax+ve	Vmax-ve
M- Control specimen	335.03	-309.23
M-XC specimen	295.82	-318.65
M-CXC specimen	400.76	-349.45
M-P specimen	284.55	-312.52
M-CXP specimen	353.11	-339.02

FIGURE 19 Decrease of the maximum base shear strength in relation to the drift ratio (after the peak).

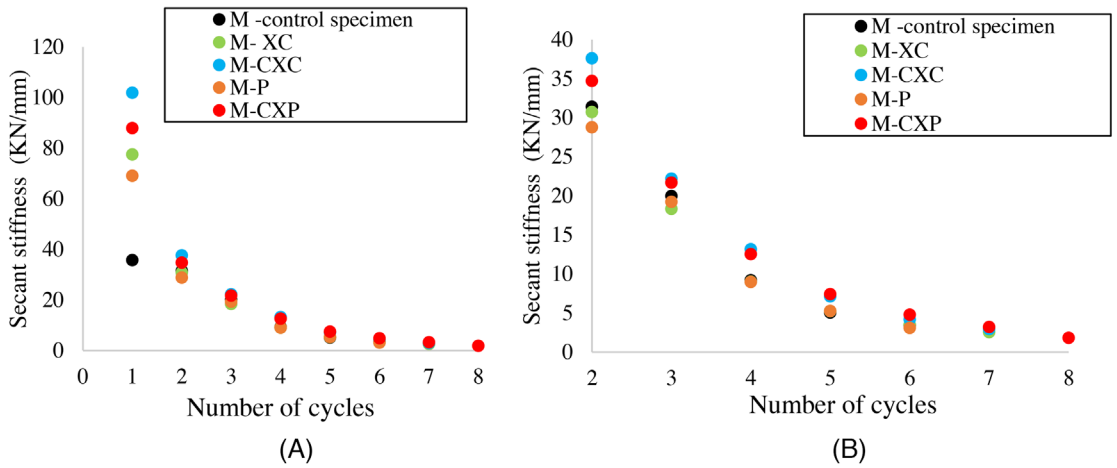

FIGURE 20 (A) Global secant stiffness in relation to the number of cycles of loading for all specimens and (B) global secant stiffness in relation to the number of cycles of loading after the second cycle of loading for all specimens.

$|-V_{max,-ve}|$ is the absolute value of the negative peak base-shear as presented in Table 3 value of i^{th} cycle and $|-X_{\max,-ve}|$ is the absolute value of displacement corresponding to the negative peak base-shear of the of i^{th} cycle.

Figure 21 shows the dissipated energy in relation to the number of half cycles of loading. The area enclosed by each hysteresis loop in the base-shear versus displacement diagram is the energy dissipated at each cycle of loading. Using a simple calculation, the evolution of the dissipated energy is expressed by Equation (2):

$$S_i = S_{i-1} + 0.5 * \left(V_{b,i} + V_{b,i-1}\right) * \left(X_{b,i} - X_{b,i-1}\right) \quad (2)$$

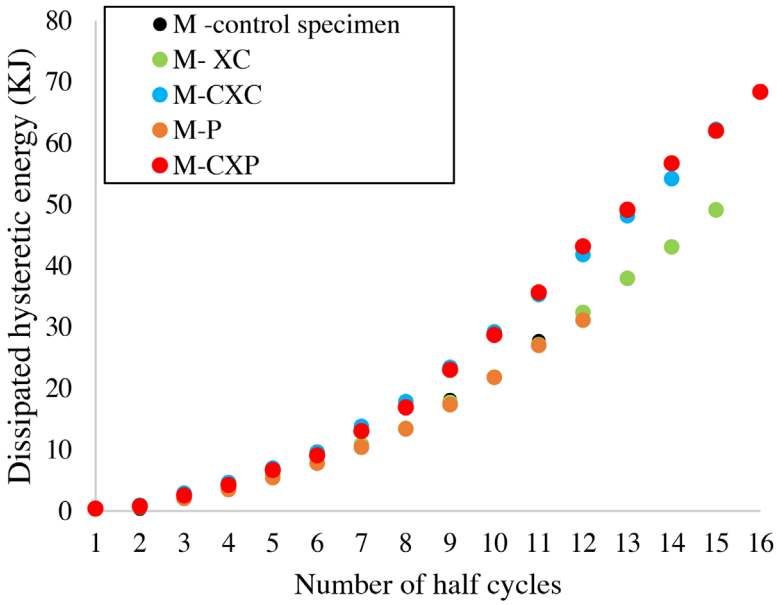

FIGURE 21 Dissipated energy in relation to the number of half-cycles of loading for all specimens.

where $(V_{b,i}, V_{b,i-1})$ is the base-shear in two consecutive points of the loading and the $(X_{b,i}, X_{b,i-1})$ is the corresponding displacement.

From Figure 20A it is observed that the initial stiffness of the infilled frame is increased by applying either one layer or two layers of TRM. The initial stiffness of the M-CXC specimen, (green dots in Figure 20) and of the M-CXP specimen (red dots in Figure 20) is increased by about 185% and 94%, respectively, compared to that of the un-retrofitted specimen (control specimen, black dots in Figure 20). The initial stiffness of M-XC specimen (blue dots in Figure 20) and of the M-P specimen (yellow dots in Figure 20) is increased by 74% and 46%, respectively, compared to that of the un-retrofitted specimen. From Figure 20B it is observed that after the second cycle of loading which corresponds to 0.35% drift ratio, the secant stiffness of the M-XC specimen (green dots in Figure 20B) is almost the same as that of the un-retrofitted infilled frame (M-control specimen, black dots in Figure 20B) except at the third cycle of loading (which correspond at 0.53% drift ratio) where the secant stiffness of the unretrofitted specimen is slightly larger than that of the M-XC specimen. Also, from the second cycle of loading (which correspond to 0.35% drift ratio) and until the fourth cycle of loading (which corresponds to 0.89% drift ratio), the secant stiffness of M-CXC specimen (blue dots in Figure 20B) and of the M-CXP specimen (red dots in Figure 20B) is increased by about 11%−43% and by 5%−43% compared to that of the unretrofitted specimen. After the fourth cycle of loading until the end of the test the secant stiffens for all the specimens is almost the same and equal to that of the bare frame due to the failures that occurred in the infill walls.

From Figure 21 it is observed that at early stages of lateral loading (up to 0.53% drift ratio, which corresponds to six half cycles of loading) the dissipated energy is almost the same for all the specimens After the 0.53% drift ratio the dissipated energy of the M-CXC specimen (green dots in Figure 21) and that of the M-CXP specimen, (red dots in Figure 21) is increased by 13%−63% and 20%−30%, respectively, compared to that of unretrofitted specimen (M-control specimen with black dots in Figure 21).

5 | CONCLUSIONS

In this paper part of the experimental campaign in the framework of the SupERB research project aiming to investigate the efficiency of integrated seismic and energy upgrading systems is presented. The integrated approach is based on the use of TRM overlays combined either with traditional thermal insulation, XPS, or with thermally efficient mortar incorporating PCMs. In that project, a series of tests for examining the energy performance of various retrofitting solutions were also carried out, along with the formulation of a methodology for the selection of the best solution for integrated seismic and energy upgrading for a given structure. In this paper, only the structural performance of masonry-infilled RC frames retrofitted with the proposed integrated approach is presented, while the energy benefits will be presented in a separate paper.

In this study, the structural performance of an integrated seismic and energy upgrading approach was assessed through full-scale in-plane loading tests on retrofitted masonry-infilled RC frames. The solutions examined are based on the use of

TRM overlays constructed using both conventional polymer-modified cement mortar combined with traditional thermal insulation composed of XPS boards, and a purposely developed thermally efficient cementitious mortar incorporating microencapsulated PCMs, which was providing both thermal and structural upgrading. The proposed integrated approach can be applied on the exterior face of the structure, so as to facilitate its application in real structures in the easiest possible way and with minimum disturbance to the inhabitants of the buildings. Five full-scale masonry-infilled RC frames that were retrofitted with different schemes of TRM combined with thermal insulation materials were subjected to in-plane displacement-controlled cyclic loading. The following parameters were investigated experimentally: the number of TRM overlays (one or two layers of TRM combined with thermal insulation), the use of thermally efficient PCM-enhanced TRM layer in contrast to the use of conventional XPS insulation, and different retrofitting configurations (placement of the TRM in a sandwich form over and/or under the novel or the traditional insulation). From the results obtained in this study the following main conclusions are derived:

1. One-sided application of either one layer of TRM or two layers of TRM on infilled RC frames contributes to better distribution of cracks and to the delay of brittle failures of the frame elements. It also remained intact throughout the tests preventing the fall of debris out of the plane of the infilled frame. Using two instead of one TRM layers can further improve crack distribution, can prevent damage localization, and can reduce the width of the cracks.
2. The TRM strengthening was found to increase the displacement capacity of infilled frames since in the case of using two layers of TRM (with or without PCMs) the displacement capacity is equal to a 2.85% drift ratio which represents an increase equal to 45% compared to the unretrofitted one.
3. The lateral resistance of retrofitted masonry-infilled RC frames up to a 0.25% drift ratio is increased regardless of the retrofitting scheme. This increase in the lateral resistance is more pronounced in the case of two layers of TRM since at this stage the lateral resistance is increased by an average of 20% compared to the infilled frames retrofitted with one layer of TRM and by 100% compared to the unretroffited one.
4. The use of two layers of TRM resulted in an increase to the maximum lateral resistance of 15%−20% compared to the unretroffited one, at the corresponding drift ratio equal to 0.35%.
5. The proposed PCM-enhanced TRM was also found to contribute to a better distribution of cracks and to delay the failures that occurred in the infilled frame without retrofitting. However, the observed increase in lateral resistance was relatively small.
6. The response of the infilled frame retrofitted with one layer of TRM with or without PCMs is almost the same with the unretrofitted one after the maximum lateral resistance is reached. On the other hand, at this stage, the lateral resistance of infilled frames retrofitted with two layers of TRM increases by 35% compared to that of the unretrofitted and by 30% for the retrofitted with one layer of TRM, and this increase is maintained for large displacements.

From the above, it can be concluded that all energy and seismic upgrading systems examined in this study have a positive impact in the response of the structural system to cyclic loading, with the ones with two layers of TRM having a better performance compared to the ones with one layer of TRM and all of them a better performance than the control specimen. The use of two layers of TRM cancels the drawback of infilled frames, which at very small drifts they reach their maximum capacity and after that they rapidly fall to the capacity of the bare frame, providing capacities above 80% of their peak capacity for drifts up to 2%. In all the tests the TRM whether it was combined with XPS or included PCMs contributed to a better distribution of the cracks in the infill and delayed premature brittle failures, although it was placed only on one side of the infill, to simulate the application to a real structure.

The proposed integrated approach can be applied on the exterior face of the structure, so as to facilitate its application in real structures in the easiest possible way and with minimum disturbance to the inhabitants of the buildings. The philosophy behind this retrofitting method is that it will provide confinement to buildings by wrapping the TRM all around the structure with adequate anchorage length at places where a connection should be made. In addition, by applying the TRM combined with XPS or included PCMs all around the structure, as it is proposed in this study, circumferential confinement is provided that results in hoop stresses that may contribute to preventing also the out-of-plane failure of the walls since in this study the TRM remained intact throughout the tests preventing the fall of debris out of the plane of the infilled frame both in the retrofitted and unretrofitted sides. This indicates that the need for anchors may be reduced, but further testing is needed to quantify this. Thus, further experimental and numerical studies are needed to examine the parameters influencing the proposed integrated retrofitting system. To examine the behavior of this system in multi-story multi-bay structures without performing experimental tests, which have high cost, the results presented in this study will be used for numerical simulations. Considering the limited research regarding the effectiveness of using TRM combined

with thermal insulation materials for integrated seismic and energy upgrading of existing buildings, further research is required as it is a new and emerging field.

ACKNOWLEDGMENTS

The work presented in this paper has been undertaken in the framework of the research project "Novel integrated approach for seismic and energy upgrading of existing buildings" SupERB (INTEGRATED/ 0916/0004), which is co-funded by the Cyprus Research and Innovation Foundation and the European Regional Development Fund, under the Integrated Projects call of the "RESTART 2016–2020" Programme for Research, Technological Development and Innovation".

DATA AVAILABILITY STATEMENT

The data that support the findings of this study are available on request from the corresponding author. The data are not publicly available due to privacy or ethical restrictions.

ORCID

Filippou Christiana A https://orcid.org/0000-0003-2798-8998

REFERENCES

1. EC. Directive of the european parliament and of the council on the energy performance of buildings (recast)COM(2021) 802 final, 2018.
2. Calvi GM, Sousa L, Ruggeri C. Energy efficiency and seismic resilience: a common approach. *Multi-Hazard Approaches to Civil Infrastructure Engineering*. Springer International Publishing; 2016. doi:10.1007/978-3-319-29713-2_9
3. Sajn N. Energy Efficiency of Buildings: A Nearly Zero-Energy Future. European Parliamentary Research Service, European Union. 2019.
4. Marini A, Passoni C, Belleri A, et al. Combining seismic retrofit with energy refurbishment for the sustainable renovation of RC buildings: a proof of concept. *Eur J Environ Civil Eng*. 2022;26(7):2475-2495. doi:10.1080/19648189.2017.1363665
5. European Committe. The European Green Deal. Brussels, 11.12.2019, COM(2019)640. 2019.
6. EC A. Renovation Wave for Europe – greening our buildings, creating jobs, improving lives, COM (2020). 2020.
7. Filippou C, Furtado A, De Risi MT, Kyriakides N, Chrysostomou CZ. Behaviour of masonry-infilled RC frames strengthened using textile reinforced mortar: an experimental and numerical studies overview. *J Earthq Eng*. 2022;00(00):1-25. doi:10.1080/13632469.2021.1988763
8. Koutas L, Triantafillou T, Bousias S. Seismic strengthening of masonry-infilled RC frames with TRM: experimental study. *J Compos Constr*. 2014;19(2):04014048. doi:10.1061/(ASCE)CC.1943-5614.0000507
9. Pohoryles DA, Bournas DA. Seismic retrofit of infilled RC frames with textile reinforced mortars: state-of-the-art review and analytical modelling. *Compos Part B Eng*. 2020;183:107702. doi:10.1016/j.compositesb.2019.107702
10. Akhoundi F, Vasconcelos G, Lourenço P, Silva LM, Cunha F, Fangueiro R. In-plane behavior of cavity masonry infills and strengthening with textile reinforced mortar. *Eng Struct*. 2018;156:145-160. doi:10.1016/j.engstruct.2017.11.002
11. Filippou Christiana A, Kyriakides NC, Chrysostomou CZ. Numerical study of the seismic retrofitting of masonry-Infilled RC frames with openings using TRM. *Earthq Eng Struct Dyn*. 2023;52:776-805. doi:10.1002/eqe.3787
12. Minotto M, Verlato N, Donà M, da Porto F. Strengthening of in-plane and out-of-plane capacity of thin clay masonry infills using textile- and fiber-reinforced mortar. *J Compos Constr*. 2020;24(6). doi:10.1061/(asce)cc.1943-5614.0001067
13. Kariou FA, Triantafyllou SP, Bournas DA, Koutas LN. Out-of-plane response of masonry walls strengthened using textile-mortar system. *Constr Build Mater*. 2018;165:769-781. doi:10.1016/j.conbuildmat.2018.01.026
14. Sagar S, Singhal V, Durgesh C, Rai M. In-plane and out-of-plane behavior of masonry-infilled RC frames strengthened with fabric-reinforced cementitious matrix. *ASCE J Struct Eng*. 2019;23(1).
15. De Risi M, Furtado A, Rodrigues H, Melo J, Verderame G, Arêde A. Experimental analysis of strengthening solutions for the out-of-plane collapse of masonry infills in RC structures through textile reinforced mortars. *Eng Struct*. 2020;27(110203):1-118.
16. Furtado A, Rodrigues H, Arêde A, Varum H. Out-of-plane behavior of masonry infilled RC frames based on the experimental tests available: a systematic review. *Constr Build Mater*. 2018;168:831-848. doi:10.1016/j.conbuildmat.2018.02.129
17. Furtado A, Rodrigues H, Arêde A, Varum H. Experimental evaluation of out-of-plane capacity of masonry infill walls. *Eng Struct*. 2016;111:48-63. doi:10.1016/j.engstruct.2015.12.013
18. Ismail N, El-maaddawy T, Khattak N. Quasi-static in-plane testing of FRCM strengthened non-ductile reinforced concrete frames with masonry infills. *Constr Build Mater*. 2018;186:1286-1298. doi:10.1016/j.conbuildmat.2018.07.230
19. Jelle BP. Traditional, state-of-the-art and future thermal building insulation materials and solutions – Properties, requirements and possibilities. *Energy Build*. 2011;43(10):2549-2563. doi:10.1016/j.enbuild.2011.05.015
20. Schiavoni S, D'Alessandro F, Bianchi F, Asdrubali F. Insulation materials for the building sector: a review and comparative analysis. *Renew Sustain Energy Rev*. 2016;62:988-1011. doi:10.1016/j.rser.2016.05.045
21. Triantafillou TC, Karlos K, Kefalou K, Argyropoulou E. An innovative structural and energy retrofitting system for URM walls using textile reinforced mortars combined with thermal insulation: mechanical and fire behavior. *Constr Build Mater*. 2017;133:1-13. doi:10.1016/j.conbuildmat.2016.12.032

22. Karlos K, Tsantilis A, Triantafillou T. Integrated seismic and energy retrofitting system using textile-reinforced mortars combined with thermal insulation. *Lecture Notes Civil Eng*. 2022;198 LNCE:3-18. doi:10.1007/978-3-030-88166-5_1
23. Gkournelos PD, Bournas DA, Triantafillou TC. Combined seismic and energy upgrading of existing reinforced concrete buildings using TRM jacketing and thermal insulation. *Earthq Struct*. 2019;16(5):625-639. 10.12989/eas.2019.16.5.625
24. Facconi L, Lucchini SS, Minelli F, Grassi B, Pilotelli M, Plizzari GA. Innovative method for seismic and energy retrofitting of masonry buildings. *Sustainability (Switzerland)*. 2021;13(11):1-21. doi:10.3390/su13116350
25. Bournas DA. Concurrent seismic and energy retrofitting of RC and masonry building envelopes using inorganic textile-based composites combined with insulation materials: a new concept. *Compos Part B Eng*. 2018;148:166-179. doi:10.1016/j.compositesb.2018.04.002
26. Bournas D. Innovative Materials for Seismic and Energy Retrofitting of the Existing EU Buildings. 2018.
27. Manganelli B, Mastroberti M, Vona M. *Evaluation of Benefits for Integrated Seismic and Energy Retrofitting for the Existing Buildings*. Springer International Publishing; 2019;101:654-662. doi:10.1007/978-3-319-92102-0_71
28. Pohoryles DA, Maduta C, Bournas DA, Kouris LA. Energy performance of existing residential buildings in Europe: a novel approach combining energy with seismic retrofitting. *Energy Build*. 2020;223:110024. doi:10.1016/j.enbuild.2020.110024
29. de Sousa C, Barros JAO, Ramôa Correia J, Valente TDS. Development of sandwich panels for multi-functional strengthening of RC buildings: characterization of constituent materials and shear interaction of panel assemblies. *Constr Build Mater*. 2021;267:120849. doi:10.1016/j.conbuildmat.2020.120849
30. Bahrar M, Djamai ZI, EL Mankibi M, Si Larbi A, Salvia M. Numerical and experimental study on the use of microencapsulated phase change materials (PCMs) in textile reinforced concrete panels for energy storage. *Sustain Cities Soc*. 2018;41:455-468. doi:10.1016/j.scs.2018.06.014
31. Baek E, Pohoryles DA, Kallioras S, Bournas DA, Choi H, Kim T. Innovative seismic and energy retrofitting of wall envelopes using pre-fabricated textile-reinforced concrete panels with an embedded capillary tube system. *Eng Struct*. 2022;265:114453. doi:10.1016/j.engstruct.2022.114453
32. Eurocode 2 British Standard. *Eurocode 2: Design of Concrete Structures*. 2008.
33. https://tsircon.com/product/tsirco-poly-122-122l/
34. Illampas R, Rigopoulos I, Ioannou I. Influence of microencapsulated Phase Change Materials (PCMs) on the properties of polymer modified cementitious repair mortar. *J Build Eng*. 2021;40:102328. doi:10.1016/j.jobe.2021.102328
35. Risi MTD, Rodrigues H. Assessment of strengthening solutions for the out-of-plane collapse of masonry infills through textile reinforced mortars: 1–11.
36. Koutas LN, Bournas DA. Out-of-plane strengthening of masonry-infilled RC frames with textile-reinforced mortar jackets. *J Compos Constr*. 2018;23(1):04018079. doi:10.1061/(asce)cc.1943-5614.0000911
37. Filippou CA, Chrysostomou CZ. Analytical model for textile reinforced mortar under monotonic loading. *Constr Build Mater*. 2020;258:120178. doi:10.1016/j.conbuildmat.2020.120178
38. Filippou CA. Numerical study on the seismic retrofitting of masonry-infilled RC frames using textile-reinforced mortar. 2021. https://hdl.handle.net/20.500.14279/23315
39. Filippou CA, Kyriakides NC, Chrysostomou CZ. Numerical modelling and simulation of the in-plane response of a three-storey masonry-infilled RC frame retrofitted with TRM. *Adv Civil Eng*. 2020:1-19. doi:10.1155/2020/6279049
40. Filippou CA, Kyriakides NC, Chrysostomou CZ. Numerical modeling of masonry-infilled RC frame. The open construction and building. *Technol J*. 2019;13(1):3-16. doi:10.2174/187483680191301
41. Filippou CA, Kyriakides NC, Chrysostomou CZ, Effect of connection detail at interface of masonry-. The 17th World Conference on Earthquake Engineering 17th, Sendai, Japan; 2020.

How to cite this article: Christis Z C, Renos V, Nicholas K, Rogiros I, Christiana A F, Stathis B. Seismic and energy upgrading of existing buildings—full-scale testing of retrofitted masonry-infilled RC frames. *Earthquake Engng Struct Dyn*. 2023;1-29. https://doi.org/10.1002/eqe.3965